Break-induced replication is activated to repair R-loop-associated double-strand breaks in SETX-deficient cells

Tong Wu[1], Youhang Li[1], Linda Z. Shi[2], and Xiaohua Wu[1,*]

[1]Department of Molecular and Cell Biology, The Scripps Research Institute, La Jolla, CA 92037

[2]The Institute of Engineering in Medicine, University of California, San Diego, California 92093

[*]The Correspondence Author

Telephone: 858-784-7910, Fax: 858-784-7978, email: xiaohwu@scripps.edu

Running title: Hyper BIR in SETX-deficient cells

Key words: Senataxin (SETX), R-loop, double-strand break (DSB), Break-induced replication (BIR), homologous recombination (HR), end resection, template switching, PIF1, MRE11, XPF, RAD52

Abstract

The primary role of Break-induced replication (BIR) is thought to be repairing single-ended double-strand breaks (seDSBs) generated at broken replication forks and eroding telomeres. In this study, we demonstrated that when senataxin (SETX), an RNA/DNA helicase, is defective, hyperrecombination using the BIR mechanism is induced at R-loop-accumulated double-ended double-strand breaks (deDSBs), suggesting a potential role of BIR in repair of R-loop-associated deDSBs. Intriguingly, loss of SETX initiates a non-canonical hyper end resection pathway requiring RAD52 and XPF, which in turn causes accumulation of PCNA and PIF1, a key player for BIR, to R-loop-associated deDSBs to establish BIR. Strikingly, SETX-deficiency does not only induce hyper BIR, but also causes a drastic increase of template switching during BIR, which has a potential to induce complex chromosome rearrangements. Additionally, SETX is synthetic lethal with RAD52 and PIF1. Collectively, our work uncovers a pivotal new function of SETX in modulating BIR to safeguard genome integrity, sheds light on how R-loops influence the utilization and fidelity of DSB repair pathways and offers new strategies for targeted treatment of SETX-deficient tumors.

Introduction

DNA double strand breaks (DSBs) represent the most dangerous form of DNA damage, which could lead to genome instability and, more severely, to cell death (Khanna & Jackson, 2001). DSBs can be repaired by two major pathways; homologous recombination (HR) and non-homologous end joining (NHEJ) (Jackson & Bartek, 2009). Homology-dependent HR serves as an error-free mechanism to repair DSB, whereas homology-independent NHEJ could be error-prone in some cases (Ceccaldi *et al*, 2016). While NHEJ remains active throughout the cell cycle, HR is activated when cells enter S and G2 phases when sister chromatids are available to serve as templates (Hustedt & Durocher, 2016). Break-induced replication (BIR) is a subtype of HR, which operates at one-ended DSBs, such as collapsed replication forks and eroding telomeres (Liu & Malkova, 2022; Quinet *et al*, 2017; Sobinoff & Pickett, 2017). BIR and HR share similar initiation steps, including end resection and strand invasion, but diverge at the DNA synthesis step, where BIR exhibits a much longer DNA synthesis tract than HR (Kramara *et al*, 2018; Sakofsky & Malkova, 2017). To achieve long-tract DNA synthesis, BIR employs a unique feature distinct from HR; BIR replication is dependent on POLD3/Pol32, a subunit of DNA polymerase δ, and helicase PIF1 (Buzovetsky *et al*, 2017; Li *et al*, 2021b; Wilson *et al*, 2013). It is also noteworthy that BIR forks often are unstable, disassociating from the original templates and reinvading the same sites or dispersed repeated sequences elsewhere in the genome (Smith *et al*, 2007). This phenomenon is called template switching and can generate complex chromosome rearrangements (Kramara *et al.*, 2018; Pardo & Aguilera, 2012). It has also been reported that the mutation frequency associated with BIR is significantly higher than that of S-phase DNA replication (Deem *et al*, 2011). Given the highly mutagenic nature of BIR, delicate regulation pathways have been described to restrict BIR activation in yeast (Liu *et al*, 2021; Pham *et al*, 2021), while analogous mechanisms await to be explored in mammalian cells.

R-loops are three-stranded nucleic acid structures formed by extended annealing of nascent RNA to the DNA template, composing an RNA/DNA hybrid and displaced single-strand DNA (ssDNA). While R-loops possess important biological functions such as transcription regulation, DNA repair, mitochondrial replication and maintaining telomere and centromeric integrity, their persistence can be detrimental, leading to genome instability (Garcia-Muse & Aguilera, 2019; Niehrs & Luke, 2020). Abundant evidence has suggested that R-loops are induced at DSB sites and actively involved in DSB repair (Brickner *et al*, 2022; Marnef & Legube, 2021; Petermann *et al*, 2022), but a comprehensive understanding of the underlying mechanisms is still elusive and under debate. On one hand, it has

been proposed that forming RNA/DNA hybrids at DSB ends interferes with the repair process. For instance, upon loss of R-loop resolution factors DDX5, DHX9, and HNRNPD, hybrids accumulate at induced DSBs, which impede end resection, causing diminished RPA and RAD51 loading and defective HR (Alfano *et al*, 2019; Matsui *et al*, 2020; Sessa *et al*, 2021; Yu *et al*, 2020). While these studies suggest that hybrids at DSBs suppress end resection, inactivation of EXOSC10, an exosome catalytic subunit, which leads to increased hybrid levels, strongly stimulates end resection, despite HR still being suppressed due to impaired RPA recruitment (Domingo-Prim *et al*, 2019). Conversely, RNA/DNA hybrids at DSBs have also been found to promote DSB repair by HR. DSB-induced small RNAs (diRNAs) and damage-induced long non-coding RNA (dilncRNA) facilitate the recruitment of HR proteins such as BRCA1, BRCA2 and RAD51 to DSBs (D'Alessandro *et al*, 2018; Gao *et al*, 2014; Michelini *et al*, 2017). Additionally, in G2 cells exposed to IR, RAD52 is recruited to DNA damaging sites in a transcription and R-loop-dependent manner to promote HR (Yasuhara *et al*, 2018). Interestingly, in yeast, defects in forming or removing RNA/DNA hybrids both impede HR efficiency, suggesting that transient RNA/DNA formation at DSBs is essential for HR (Ohle *et al*, 2016). The controversial findings in the repair outcomes likely stem from the complex and intricate regulation exerted by R-loops/hybrids at different DSB repair steps, involving multiple players. Understanding the detailed mechanisms of how various R-loop resolving factors modulate the DSB repair process is critical for uncovering the biological significance of R-loops/hybrids at DSB ends.

SETX encodes a putative RNA-DNA helicase capable of unwinding RNA-DNA hybrids and plays an important role in R-loop homeostasis (Gatti *et al*, 2023; Giannini & Porrua, 2024; Groh *et al*, 2017). Human SETX defects are documented in the neurodegenerative disorder ataxia with oculomotor apraxia 2 (AOA-2) (Moreira *et al*, 2004) and autosomal dominant amyotrophic lateral sclerosis type 4 (ALS4) (Chen *et al*, 2004). Substantial evidence suggests an important role of SETX in the maintenance of genome stability (Gatti *et al.*, 2023; Giannini & Porrua, 2024; Groh *et al.*, 2017). SETX and its yeast orthologue Sen1 interact with RNA Pol II (Chen *et al*, 2006; Suraweera *et al*, 2009; Ursic *et al*, 2004) and are involved in transcription regulation and termination (Gatti *et al.*, 2023; Giannini & Porrua, 2024). SETX and Sen1 associate with replication forks, promoting replication through transcription active genes (Alzu *et al*, 2012). SETX forms foci colocalizing with DNA repair proteins upon replication stress and is believed to participate in resolving transcription and transcription conflict (TRC) (Richard *et al*, 2013; Yuce & West, 2013). SETX in complex with BRCA1 is also involved in dismantling R-loops at transcription pause sites in transcription termination

regions to prevent DNA damage (Hatchi *et al*, 2015). Furthermore, it has been demonstrated that SETX and Sen1 are recruited to DSBs when they occur in transcriptionally active loci to limit accumulation of R-loops/RNA-DNA hybrids (Cohen *et al*, 2022; Cohen *et al*, 2018; Hatchi *et al.*, 2015; Rawal *et al*, 2020). Importantly, the loss of SETX and Sen1 both results in enhanced translocation by increasing illegitimate rejoining of distal DNA ends (Cohen *et al.*, 2018; Rawal *et al.*, 2020), suggesting a key role of SETX and Sen1 in resolving R-loops at DSB ends to facilitate the utilization of pathways promoting faithful DSB repair. However, the underlying mechanisms of how accumulated R-loops/hybrids associated with SETX/Sen1 deficiency lead to the change of repair pathway usage, resulting in deleterious chromosomal rearrangements, remain elusive.

In this study, by using EGFP-based reporters, which specifically monitor HR and BIR pathways in mammalian cells (Li *et al.*, 2021b), we found a significant increase in both HR and BIR when SETX is deficient. Interestingly, short tract gene conversion (STGC), which is usually referred to as HR, alters its genetic dependence in SETX-deficient cells and shows characteristics of BIR, requiring PIF1 and POLD3. End resection is substantially stimulated in an R-loop-dependent manner at DSBs when SETX is deficient, leading to the onset of BIR mechanism for homology-directed repair. This hyper end resection is initiated by RAD52/XPF-mediated cleavage, distinct from the canonical end resection pathway which involves CtIP and the endonuclease activity of MRE11. Furthermore, by analyzing BIR repair products, we observed a substantial elevation of template switching during BIR in SETX-deficient cells, providing insights into the mechanisms to generate replicative insertions and chromosomal rearrangements that are often present in cancer genomes.

Results

SETX loss induces hyperrecombination for both HR and BIR in an R-loop-dependent manner.

In our previous study, we established EGFP-based reporter systems to determine the efficiency of DSB repair mediated by the HR (STGC) pathway (Fig 1A) and the BIR (long tract gene conversion: LTGC) pathway (Fig 1B) (Li *et al.*, 2021b). In yeast, gene conversion with tract length longer than 1 kb, uses the BIR mechanism (Jain *et al*, 2009; Mehta *et al*, 2017). In our EGFP-BIR reporter (Li *et al.*, 2021b), if BIR DNA synthesis continues for 3.8 kb, reaching the homology outside of the reporter on the right side of the break, BIR is completed by synthesis-dependent strand annealing (SDSA, BIR-SDSA), whereas if the BIR synthesizing strand is prematurely disassociated from its template and is ligated to the other side of the break, BIR is completed by end joining (BIR-EJ) (Fig S1A). As long as

BIR DNA synthesis proceeds sufficiently to complete the FP region, green cells can be produced. Therefore, the gene conversion tract length ranges from 1.2 to 3.8 kb for BIR-EJ and is 3.8 kb or longer for BIR-SDSA (Li *et al.*, 2021b). We showed that both BIR-SDSA and BIR-EJ depend on POLD3 and PIF1 (Li *et al.*, 2021b).

Interestingly, we found that SETX depletion or knockout (KO) results in a significantly higher percentages of GFP-positive cells in both U2OS (EGFP-HR) and U2OS (EGFP-BIR) reporter cell lines after I-SceI cleavage (Fig 1C and 1D), suggesting that SETX deficiency induces hyperrecombination for both HR and BIR. To determine whether the helicase activity of SETX is required for suppressing hyperrecombination, we expressed SETX wildtype (WT) allele or helicase-dead mutant SETX-P-loopΔ, containing deletion of eight amino acids (Δ1963-1970aa) in the SETX P-Loop GTP/ATP binding motif (Bennett *et al*, 2020) in both WT and *SETX*-KO U2OS (EGFP-BIR) reporter cells. While expressing the SETX-WT allele suppresses hyper BIR in *SETX*-KO cells, the helicase-dead mutant failed to do so (Fig 1E). Consistent with the role of SETX in resolving R-loops (Crossley *et al*, 2023; Zhao *et al*, 2022), we showed stronger R-loop staining in *SETX*-KO cells compared to WT cells, with RNASEH1 overexpression attenuating the increase (Fig 1F). Overexpression of RNASEH1 in SETX-depleted cells also leads to suppression of hyperrecombination for BIR (Fig 1G) and HR (Fig 1H). These results suggest that SETX deficiency promotes hyperrecombination for both HR and BIR in an R-loop-dependent manner.

HR in SETX-deficient cells resembles BIR.

It has been well established that PIF1 helicase is required for BIR (LTGC) but is dispensable for HR (STGC) (Li *et al.*, 2021b). We showed that both BIR and hyper BIR induced by SETX depletion are strongly impaired in *PIF1*-KO cells, confirming the use of BIR (Fig 2A). Interestingly, however, while HR in SETX-proficient cells is not dependent on PIF1, depleting PIF1 in *SETX*-KO cells leads to a significant reduction of HR, suggesting that PIF1 is required for HR in SETX-deficient cells (Fig 2B and Fig S1B). This suggests that SETX deficiency disrupts the regulation of the onset of HR and BIR and promotes the establishment of using the BIR mechanism even for HR/STGC. To investigate how the BIR mechanism is established at DSBs for HR/STGC, we monitored the recruitment of EGFP-tagged PIF1 to laser-induced damaged sites in both WT and *SETX*-KO cells. As depicted in Fig 2C, recruitment of EGFP-PIF1 to DSBs is significantly increased in *SETX*-KO cells compared to WT cells. We speculate that enhanced PIF1 recruitment to DSBs in SETX-deficient cells may facilitate the

onset of the BIR mechanism for DSB repair.

SETX plays multiple roles in preventing DSB formation and genome instability (Gatti *et al.*, 2023; Giannini & Porrua, 2024; Groh *et al.*, 2017). Consistently, depletion of SETX results in a significant increase γ-H2AX foci formation, which can be suppressed by RNASEH1 overexpression (Fig 2D). Based on our observation that SETX deficiency results in hyperrecombination, which is dependent on PIF1 for both BIR and HR, we reason that repair of DSBs spontaneously formed in SETX-deficient cells would heavily rely on PIF1. Indeed, γ-H2AX is significantly increased in cells depleted for both PIF1 and SETX (Fig 2E), and SETX and PIF1 exhibit synthetic lethal interactions (Fig 2F). Collectively, we conclude that hyperrecombination induced in SETX-deficient cells primarily occurs through activating the BIR mechanism rather than HR, and that BIR becomes an essential DSB repair pathway for the survival of SETX-deficient cells.

SETX loss induces excessive end resection mediated by a non-canonical pathway.

The impact of accumulated R-loops on DSB repair often involves the regulation of end resection (Alfano *et al.*, 2019; Domingo-Prim *et al.*, 2019; Matsui *et al.*, 2020; Sessa *et al.*, 2021; Yu *et al.*, 2020). To investigate the effect of SETX loss on end resection, we first examined the level of RPA2 phosphorylation at S4 and S8 (pRPA2) after ionizing radiation (IR), known to be induced by end resection (Liaw *et al*, 2011). As shown in Fig 3A, *SETX*-KO cells manifest stronger pRPA2 signal up to 4 hours after IR compared to WT cells, indicative of overactive end resection. We further performed the well-established quantitative end resection assay (Zhou *et al*, 2014) and demonstrated that end resection is significantly enhanced in *SETX*-KO cells at I-SceI-induced DSBs in the BIR reporter (Fig 3B). Additionally, recruitment of EGFP-RPA2 to the laser-induced damage sites is also enhanced in *SETX*-KO cells compared to WT cells (Fig 3C), further supporting the hyper-resection phenotype in SETX-deficient cells.

By examining the binding of the RNASEH1-D210N catalytic mutant via chromatin immunoprecipitation (ChIP) as described (Chen *et al*, 2017), we showed that R-loops are indeed accumulated at the I-SceI-induced DSBs in our BIR reporter (Fig 3D). Overexpression of RNASEH1 suppresses hyper-resection observed in SETX-depleted cells (Fig 3E), as well as the increased pRPA2 level observed in *SETX*-KO cells following IR (Fig 3F), supporting the conclusion that hyper-resection in SETX-deficient cells is induced by accumulated R-loops.

To investigate how end resection leads to hyper BIR in SETX-deficient cells, we performed BIR

assay after depleting MRE11 or CtIP. While BIR is impaired in SETX-proficient cells after depletion of CtIP or MRE11, surprisingly, BIR in *SETX*-KO cells is impeded only after depletion of MRE11 but not CtIP (Fig 4A and Fig S2A and S2B). We also found that hyper-resection observed in *SETX*-KO cells is largely dependent on MRE11 but not CtIP (Fig 4B). Similar dependence on MRE11 but not CtIP was observed for the IR-induced pRPA2 level (Fig 4C). It is well established that the MRE11-RAD50-NBS1 (MRN) complex initiates the end resection by using the endonuclease activity of MRE11 to make a nick on the 5' strand with some distance from the break end, followed by using the MRE11 3' to 5' exonuclease activity to degrade DNA from the nick towards the DSB end (Cejka & Symington, 2021; Deshpande *et al*, 2016; Shibata *et al*, 2014) (Fig S2C). It has been shown that CtIP is important for stimulating the MRE11 endonuclease activity (Anand *et al*, 2019; Anand *et al*, 2016; Cannavo & Cejka, 2014; Zdravkovic *et al*, 2021). The dispensable role of CtIP for hyper-resection in SETX-deficient cells implies that the initial MRN-mediated endonuclease cleavage at DSB ends may not be involved. To test this possibility, we used an inhibitor PFM01 that specifically inhibits the endonuclease activity of MRE11 (Shibata *et al.*, 2014). Significantly, as shown in Fig 4D, treatment with PFM01 results in a reduction of end resection in SETX-proficient cells but fails to do so in SETX-deficient cells, and instead even stimulates it, while XPF depletion still leads to reduction of end resection in the presence of PFM01 in *SETX*-KO cells but not in WT cells. On the other hand, when we used the inhibitor PFM39, which specifically inhibits the exonuclease activity of MRE11 (Shibata *et al.*, 2014), we observed a clear reduction of end resection (Fig 3E left) close to the cleavage site in both WT and *SETX*-KO cells (L1, 145 bp left to I-SceI site, Fig 3B top). However, at the site L3, which is further away from the cleavage site (L3, 2989 bp left to I-SceI site, Fig 3B top), PFM39 treatment causes a minor decrease of end resection in *SETX*-KO cells with almost no effect in WT cells (Fig 3E right), consistent with the notion that extended 5' to 3' end resection involves BLM/DNA2 and EXO1, but not the MRE11 exonuclease activity (Fig S2C). Collectively, these results suggest that the initiation of abnormal hyper end resection in SETX-deficient cells is not through the canonical pathway that requires MRE11- and CtIP-dependent endonucleolytic cleavage at DSB ends. However, the MRE11 exonuclease activity is still required for 3' to 5' strand removal towards the DSB ends (Fig 7A).

R-loop accumulation activates RAD52-XPF to initiate end resection in SETX-deficient cells.

The observation that CtIP and the MRE11 endonuclease activity is dispensable for hyper-

resection in SETX-deficient cells suggests the involvement of a non-canonical end resection mechanism. It was shown previously that flap endonucleases XPF and XPG are involved in removing R-loops (Crossley *et al.*, 2023; Sollier *et al*, 2014; Tian & Alt, 2000; Yasuhara *et al.*, 2018). We found that depleting XPF leads to reduction of BIR in *SETX*-KO cells but not in WT cells (Fig 5A, Fig S3A). However, hyper BIR induced by SETX depletion is not changed in XPG-KO cells (Fig S3B and S3C). The end resection assay also reveals that hyper-resection in SETX-deficient cells, but not normal end resection in SETX-proficient cells, is dependent on XPF (Fig 5B). It has been shown that XPF physically interacts with RAD52 (Motycka *et al*, 2004), and RAD52 is recruited to DSBs containing R-loops at transcriptionally active loci (Tan *et al*, 2020; Yasuhara *et al.*, 2018). We speculate that XPF may be recruited through the R-loop-RAD52 axis. Indeed, hyper BIR and hyper end resection induced by SETX depletion is diminished in *RAD52*-KO cells compared to WT cells (Fig 5C, 5D and S3D), suggesting a role of RAD52 in promoting hyper-resection and hyper BIR specifically when SETX is deficient. Similarly, the elevated pRPA2 level due to SETX depletion is also diminished in *RAD52*-KO and *XPF*-KO cells (Fig 5E, S3D and S3E), consistent with the role of RAD52 and XPF in hyper resection in SETX-deficient cells. In addition, we examined RAD52 foci in response to IR and found that SETX depletion causes more RAD52 foci formation, which can be suppressed by RNASEH1 overexpression (Fig 5F). Similarly, SETX depletion results in enhanced XPF foci formation following IR, and this increase is diminished in *RAD52*-KO cells (Fig 5G), suggesting that the recruitment of XPF to DSBs accumulated with R-loops is dependent on RAD52. These data support the model that RAD52 recognizes DSBs occupied by R-loops, and in turn recruits XPF to cleave R-loop-associated DSB ends to initiate a non-canonical end resection pathway.

In the canonical MRN-initiated end resection, BLM, DNA2 and EXO1 are required for further long-range end resection. We depleted BLM, DNA2 and EXO1 and found that they all are indispensable for end resection in both WT and *SETX*-KO cells, as revealed by quantitative end resection assay (Fig 4F and Fig S2D, S2E and S2F) and IR-induced RPA2 phosphorylation (Fig 4G). This suggests that BLM, DNA2 and EXO1 are also involved in the RAD52-XPF hyper end resection pathway, which is activated when R-loops are accumulated at DSBs due to SETX deficiency. We anticipate that bidirectional end resection (Cejka & Symington, 2021) with 3' to 5' by the MRE11 exonuclease activity and 5' to 3' by BLM/DNA2 and EXO1 are still employed in the RAD52-XPF hyper end resection pathway (Fig 7A).

As RAD52 and XPF are required for hyper-resection in SETX-deficient cells, we examined

whether RAD52 and XPF would exhibit synthetic lethal interactions with SETX. We found that depletion of SETX in *RAD52*- or *XPF*-KO cells significantly reduces cell viability (Fig 5H), supporting the critical role of RAD52 and XPF in repairing DSBs with accumulated R-loops at the ends.

SETX deficiency promotes template switching during BIR in an R-loop-dependent manner.

We showed that SETX loss results in a significant increase of PIF1 recruitment to DSBs (Fig 2C), thereby promoting the onset of BIR mechanism at deDSBs in SETX-deficient cells. In yeast, Pif1 interacts with PCNA and this interaction is important for promoting BIR DNA synthesis (Buzovetsky *et al.*, 2017). In mammalian cells, we showed that both PCNA and PIF1 are required for BIR (Li *et al*, 2021a). Interestingly, by performing an *in situ* proximity ligation assay (PLA), we found that not only PIF1 but also PCNA recruitment to DSBs, marked by γH2AX after IR, is significantly increased after depletion of SETX (Fig 2G, 2H, S1C and S1D). We further showed that such increased PIF1 recruitment to DSBs in SETX-deficient cells is dependent on PCNA (Fig 2I, S1E and S1F). We speculate that hyper end resection at DSBs due to SETX deficiency causes PCNA accumulation, which in turn recruits PIF1 to promote BIR.

In yeast, it has been found that BIR is often associated with template switching (Smith *et al.*, 2007), which could be mutagenic. We took advantage of our BIR reporter system which allows recovering BIR events by sorting EGFP-positive cells. We performed PCR analysis of isolated single green clones to analyze the BIR repair products (Fig S4A). Interestingly, we found that all green clones derived from WT cells can be analyzed using the PCR strategy (42 out of 42), yet fewer than half of the green clones (17/41) from *SETX*-KO cells succeeded in PCR amplification (Fig S4C). Among these resolved BIR events, we observed that 5 out of 42 events (11.9%) in WT cells and 7 out of 41 events (17.1%) have switched templates locally within the BIR reporter during BIR DNA synthesis (Fig 6A and Fig S4C). The substantial increase of local template switching observed in *SETX*-KO cells raises the possibility that BIR template switching to other chromosomes may also be high in *SETX*-KO cells, making PCR analysis challenging. To facilitate the analysis of BIR products, we adapted the linear amplification-mediated high-throughput genome-wide sequencing (LAM-HTGTS) assay (Hu *et al*, 2016) to our BIR analysis (Fig S4B). We used the right side of the I-SceI cleavage site (primer R1, Fig S4B) as the bait to identify the BIR repair junctions. LAM-HTGTS-based assay offers a simple and quick way to pinpoint the BIR repair junctions for determining BIR

synthesis tract length without involving long range PCR (e.g. F1/R1 PCR product: 3 kb for BIR-SDSA product, Fig S4A). In addition to local jumping (Fig S5Aa), LAM-HTGTS can also catch the BIR events with template switching to other genomic sites but joining back to the second end of the DSB (Fig S5Ab). These jumping-out events, although with end joining back to the cleavage sites, if containing large-sized insertions, could fail the PCR analysis strategy due to too big PCR products and complex rearrangements. LAM-HTGTS cannot recover the events with template switching to other genomic loci without ligating back to the original DSB site on the reporter (Fig S5Ac).

With LAM-HTGTS, we succeeded in identifying BIR junctions in almost all green clones (40 out of 41) derived from *SETX*-KO cells (Fig 6A). Among them, we identified two more local jumping events within the BIR reporter in *SETX*-KO cells in addition to those identified by the PCR assay [total 9 events: 7 by PCR assay and 2 by HTGTS, Fig 6A and Fig S4C]. Additionally, we found that template switching to other chromosomes is substantially increased in *SETX*-KO cells (Fig 6A and 6B). Since our HTGTS assay using the R1 primer only recovers the events joining back to the second end of the DSB (Fig S4B and S5Ab), the successful identification of the repair junctions in 40 out of the total 41 events by HTGTS suggests that almost all template switching events joining back to the original break to complete the repair without causing translocation (Fig S5Aa and S5Ab). The overall frequency of template switching (including switching within and outside of the BIR reporter) in WT cells is 14.3% (Fig 6A), which is comparable to the template switching frequency reported in yeasts (Anand *et al*, 2014; Smith *et al.*, 2007). Strikingly, *SETX*-KO cells exhibit a markedly higher template switching frequency of 53.6%, nearly four times that of WT cells (Fig 6A). Additionally, most template switching events in WT cells are restricted to local reporter regions and involve one jumping (Fig 6E and Fig S4C). In contrast, in *SETX*-KO cells, template switching often spreads to other chromosomes (Fig 6A and 6B and Fig S4C), and even local jumps within the reporter region often involve multiple rounds of copy-and-paste (Fig 6D, KO; and Fig S4C). Therefore, SETX deficiency does not only lead to hyperactive BIR, but also induces substantial more template switching, which could cause genome instability.

Transcription and associated R-loop accumulation can block BIR replication fork progression and fuel template switching (Liu *et al.*, 2021). In our BIR reporter, CMV-promoter-driven transcription occurs in the donor template (Fig 1B). We hypothesize that SETX deficiency may induce R-loop formation in the BIR donor, causing conflict of BIR replication with R-loops at transcription sites (Fig 7B). Indeed, we found that SETX depletion enhances accumulation of R-loops/hybrids in the CMV

surrounding regions in the EGFP-BIR-5085 reporter, which can be suppressed by RNASEH1 overexpression (Fig 6C). Significantly, RNASEH1 overexpression leads to a reduction of template switching frequency in *SETX*-KO cells to the level comparable to WT cells (Fig 6A and 6B), suggesting that templating switching is indeed caused by R-loop accumulation. Notably, the CMV promoter and its adjacent regions are a hot spot in the BIR reporter for initiating template switching (Fig 6D and Fig S4D), supporting the model that the collision of BIR fork with R-loops formed in the CMV and its surroundings in the BIR donor template, due to SETX deficiency, causes the disassociation of the BIR synthesizing strand from the donor to initiate template switching. In addition, we found that the overall BIR tract length is significantly increased upon RNASEH1 overexpression in both WT and *SETX*-KO cells (Fig 6E), consistent with the notion that reducing R-loop level permits more processive BIR DNA synthesis without disassociation. Collectively, these findings suggest that R-loops present on the BIR templets can disrupt BIR fork migration and induce template switching.

Discussion

In this report, we identified a new role of SETX in suppressing mutagenic BIR, contributing to the maintenance of genome stability. Mechanistically, loss of SETX causes accumulation of R-loops/RNA-DNA hybrids at DSB ends, inducing a non-canonical hyperactive end resection pathway that requires RAD52-XPF. The resulting hyper end resection activity leads to the establishment of BIR mechanism, causing hyperrecombination for both BIR (LTGC) and HR (STGC) at deDSBs. Importantly, not only BIR frequency, but also BIR-associated template switching, is significantly elevated in SETX-deficient cells. This reveals an unrecognized role of SETX in preventing replication-based complex genome rearrangements (CGRs), which are commonly observed in cancer genomes, but a mechanistic understanding is lacking.

The mechanism underlying hyper end resection in SETX-deficient cells.

We observed that in SETX-deficient cells, hyperrecombination is accompanied with hyper end resection, mediated by a non-canonical end resection pathway that is independent of the MRE11 endonuclease activity and CtIP, but requires RAD52 and XPF. In one scenario, persistence of R-loops at DSBs may inhibit the MRE11 nuclease activity, preventing the endonucleolytic cleavage to initiate end resection. This is consistent with the observation that RNA-DNA hybrids inhibit the MRE11

nuclease activity in an *in vitro* assay (Chang *et al*, 2019). Alternatively, R-loop-mediated recruitment of RAD52 and subsequent activation of XPF may override the function of MRE11 and CtIP in endonucleolytic cleavage by creating nicks more internally on the 5' strands (Fig 7A). In our study, we found that XPF, but not XPG, is involved in hyper end resection at deDSBs that are associated with R-loops in SETX-deficient cells. On the other hand, it has been shown that XPF and XPG are both involved in processing R-loops to generate DSBs and the absence of XPG increases cellular R-loop levels (Makharashvili *et al*, 2018; Sollier *et al.*, 2014; Stork *et al*, 2016). Notably, at transcriptionally active DSBs, a transcription-associated HR repair (TA-HRR) mechanism has been described, where RAD52 recognizes RNA-DNA hybrids and promotes XPG-mediated R-loop processing to initiate HR (Yasuhara *et al.*, 2018). In this study, we also observed RAD52 recruitment to DSBs in an R-loop dependent manner in SETX-deficient cells, but XPF, not XPG, is subsequently recruited by RAD52 for cleaving R-loops at deDSBs to initiate end resection (Fig 7A). The use of different endonucleases could be attributed to possible structural differences in R-loops/hybrids formed prior to DSB formation (R-loop processing), at DSBs under normal conditions (TA-HRR) or with high levels of R-loop due to loss of SETX. Alternatively, stronger R-loop formation at DSBs in SETX-deficient cells may induce specific chromatin modification and/or recruit different cofactors for endonucleases, thus modulating XPF and XPG activity differently compared to other situations involving R-loops. It is worth mentioning that in an *in vitro* R-loop cleavage assay, XPF exhibits a strong activity to cleave the 5' of R-loops, but XPG almost has no cleavage activity at the 3' of R-loops (Tian & Alt, 2000) (Fig S5B). This observation supports our model that XPF, but not XPG, acts to process the 5' strand of DSBs for promoting end resection.

Notably, in a previous study using SETX depletion, hyper end resection was not detected despite the accumulation of R-loops at DSB ends (Cohen *et al.*, 2018), and this discrepancy could be related to the level of SETX depletion. However, hyper end resection was observed in yeast Sen1-deficient cells, which is consistent with our study (Rawal *et al.*, 2020). Interestingly, hyper end resection in Sen1-deficient cells does not involve Sgs1 (BLM homologue) to unwind DNA or Exo1 to degrade DNA, but requires Mre11 and Dna2 for end processing. In the yeast Sen1-deficient model, it was proposed that the Mre11 endonuclease is involved in creating a nick to initiate end resection, followed by Dna2 cleaving long 5' flaps of ssDNA in R-loops to promote extensive end resection (Rawal *et al.*, 2020). This is different from the mechanism underlying hyper end resection in human SETX-deficient cells, of which the MRE11 endonuclease activity and CtIP are dispensable. We propose that when

SETX is deficient, RAD52 recognizes accumulated R-loops at DSBs, and recruits XPF to cleave the 5' side of R-loops on the 5' strands of DSBs to initiate end resection (Fig 7A). With anticipated multiple transcription forks at transcriptional active DSBs, XPF could make a series of cleavages on the 5' strand of a DSB, thereby robustly accelerating end resection and resulting in hyperactive end resection phenotype. The MRE11 exonuclease activity, as well as BLM/DNA2 and EXO1, are still required for bidirectional processing to complete end resection.

Establishing BIR at R-loop-accumulated DSBs in SETX-deficient cells.

Importantly, the hyperrecombination we observed in SETX-deficient cells is not merely an increase of recombination activity but involves a shift of pathway usage; upon loss of SETX, elevated HR (STGC) shows BIR characteristics, requiring PIF1 (Fig 2B). BIR is primarily involved in repairing broken replication forks and eroding telomeres, where seDSBs are generated (Kramara *et al.*, 2018; Wu & Malkova, 2021). However, since BIR is highly mutagenic, associated with template switching and hyper mutation (Sakofsky *et al*, 2012; Sakofsky *et al*, 2014; Smith *et al.*, 2007), utilization of BIR at deDSBs is regulated and restricted by multiple mechanisms as described in yeast (Pham *et al.*, 2021). In this study, we demonstrated that R-loop accumulation at DSBs overrides the control of BIR restriction at deDSBs and induces the onset of BIR mechanism. We previously showed that at broken forks, both BIR/LTGC and HR/STGC utilize the BIR mechanism, requiring PIF1 and POLD3, which differs from the repair at deDSBs generated by endonucleases, where PIF1- and POLD3-independent HR/STGC is predominantly utilized over BIR/LTGC at deDSBs (Li *et al*, 2021b). This is largely attributed to the immediate assembly of BIR replisomes upon fork breakage for seDSB repair (Fig S6A left), in contrast to the regulated assembly of BIR replisomes at deDSBs only when BIR is in needed (Fig S6A right) (Li *et al.*, 2021b). We propose that over-accumulated ssDNA due to hyper end resection in SETX-deficient cells triggers PCNA loading and subsequent recruitment of PIF1 to promote BIR replisome assembly and the establishment of BIR mechanism at dsDSBs (Fig S6B), reminiscent to BIR activation at seDSBs (Fig S6A left). In this respect, we previously found that PCNA is accumulated at fork broken sites upon replication stress and PCNA is required for BIR at seDSBs (Li *et al.*, 2021b).

The primary role of BIR is to repair seDSBs (Kramara *et al.*, 2018; Wu & Malkova, 2021). However, although being restricted, BIR is still used at deDSBs despite with lower frequency compared to HR (Li *et al.*, 2021a). It has been a long-lasting question what triggers the use of BIR at

deDSBs and what the biological importance is of utilizing BIR at deDSBs. We propose that in our SETX-deficient model system, uncontrolled accumulation of R-loops at deDSBs generates signals to induce assembly of BIR replisomes, thereby establishing the BIR mechanism for both HR (STGC) and BIR (LTGC). It is tempting to speculate that in WT cells under normal situations, R-loops occasionally form at deDSBs in the transcriptionally active regions, and those deDSBs with significantly elevated R-loops may trigger BIR, whereas the ends with normal transcription activity without forming or with low R-loops would use HR (STGC) for repair (Fig S6C). We propose that modulating R-loop formation at deDSBs could be one mechanism for regulating the selection of HR (STGC) and BIR (LTGC) at deDSBs for DSB repair. Importantly, based on this study, we propose that BIR is not only important for repairing seDSBs, but can also be involved at deDSBs in the transcriptionally active regions when R-loops are accumulated.

Upon replication stress, common fragile sites (CFSs) often fail to complete replication at the onset of mitosis due to shortage of replication origins, presence of large genes and abundant secondary structures (Glover *et al*, 2017; Li & Wu, 2020; Ozeri-Galai *et al*, 2012). Mitotic DNA synthesis (MiDAS), which utilizes BIR mechanism, is involved in completing DNA synthesis at CFSs (Bhowmick *et al*, 2023). Interestingly, R-loops also frequently accumulate at CFSs due to TRC at large genes (Helmrich *et al*, 2011). Presumably, following endonuclease cleavage of CFSs (Naim *et al*, 2013; Ying *et al*, 2013), the broken ends of under-replicated regions could either be ligated by end joining, which potentially causes big deletions on mitotic chromosomes, or by BIR-mediated MiDAS, which copies missing DNA sequences from homologous chromosomes to complete DNA replication (Bhowmick *et al.*, 2023) (Fig S7). We propose that accumulated R-loops at CFSs could serve as a signal to trigger the onset of BIR to reduce the use of end joining, thereby safeguarding genome integrity by preventing deletions.

R-loops/hybrids regulate DSB repair at multiple layers.

Our study demonstrated that loss of SETX causes R-loop accumulation at deDSBs, resulting in hyper end resection and elevated recombination. However, studies on the roles of RNA/DNA hybrids at deDSBs in end resection and HR yield quite diverse and controversial results. Functional impairment of different R-loop resolvases, leading to the accumulation of R-loops/hybrids at DSBs, has resulted in varying outcomes, including impaired end resection (Alfano *et al.*, 2019; Matsui *et al.*, 2020; Ohle *et al.*, 2016; Sessa *et al.*, 2021; Yu *et al.*, 2020), no discernible influence on end resection

(Li *et al*, 2016), or accelerated end resection [(Domingo-Prim *et al.*, 2019; Rawal *et al.*, 2020), this study]. This is likely attributed to the distinct functions of different R-loop resolvases, with their impaired activities causing variations in the structure, extent, and level of R-loops/hybrids formed at deDSBs. For instance, SETX deficiency generates R-loops at DSBs that can be efficiently recognized and cleaved by RAD52-XPF, triggering a non-canonical hyper end resection pathway, which overrides the canonical MRE11-initiated end resection pathway (Fig S8a). Loss of EXOSC10 also leads to hyper transcription-dependent end resection (Domingo-Prim *et al.*, 2019). However, when certain other hybrid resolvases are defective, accumulated R-loops/hybrids could hinder end resection by preventing MRE11 cleavage for initiating end resection or suppressing BLM unwinding activity and EXO1 nuclease activity for extended end resection (Fig S8a). Inhibition of MRE11, BLM and EXO1 by R-loops/hybrids has been suggested by *in vitro* experiments (Chang *et al.*, 2019; Daley *et al*, 2020).

Different from our results with SETX deficiency resulting in hyper recombination, it has also been shown that HR could be impaired when R-loops/hybrids are accumulated at deDSBs (Fig S8b). HR defect could be caused by impaired end resection due to over-accumulated R-loops/hybrids at DSBs, or the hybrid retention on the 3' ssDNA after end resection that prevents RPA and RAD51 loading (Alfano *et al.*, 2019; D'Alessandro *et al.*, 2018; Matsui *et al.*, 2020; Ohle *et al.*, 2016; Sessa *et al.*, 2021; Yu *et al.*, 2020). We propose that both the formation and removal of R-loops/hybrids at DSBs are critical for HR, and different hybrid resolvases potentially act at various stages to regulate HR. In addition to the role of R-loops/hybrids in modulating end resection activity, hybrid formation on the 3' strands aids in protecting the 3' ends, but it is necessary to remove hybrids afterwards to facilitate RPA and RAD51 loading for promoting strand invasion (S8c). In yeast, both depletion of Rnh1 and Rnh201 and overexpression of Rnh1 result in HR defects (Ohle *et al.*, 2016), suggesting a delicate balance in R-loops/hybrid formation for regulating HR. Regarding SETX deficiency, we propose that while accumulated R-loops in SETX-deficient cells promote hyper end resection, SETX is not directly involved in removing hybrids formed on the 3' strands, which may require other resolvases (Fig S8c). Consequently, in SETX-deficient cells, the over-resected 3' ssDNA can be accessed by RPA and RAD51 and remains capable of facilitating strand invasion, thereby promoting hyper HR and BIR. Hence, regulating the dynamics of R-loops/hybrids at DSBs at different steps could positively or negatively influence HR and regulate the selective use of HR and BIR.

The role of SETX in the maintenance of genome stability.

SETX, like its counterpart Sen1, plays an important role in the maintenance of genome stability through multiple mechanisms (Gatti *et al.*, 2023; Giannini & Porrua, 2024; Groh *et al.*, 2017). SETX prevents oxidative damage (Suraweera *et al.*, 2009) and is recruited to replication forks to resolve TRC, thereby avoiding DSB formation. SETX is also recruited by BRCA1 to transcriptional termination pausing sites to process R-loops and prevent DSB formation (Hatchi *et al.*, 2015). Our study reveals another important role of SETX in preventing replication-associated genomic rearrangements through suppressing template switching during BIR. Strikingly, BIR template switching is increased more than four-fold in SETX-deficient cells, with multiple template-jumping events even in a single BIR event. When deDSBs are generated in transcriptionally active regions, BIR could be activated due to R-loop formation at DSB ends. Additionally, the BIR templates, usually on the sister chromatids, are also expected to be transcriptional active, and SETX is required for resolving R-loops on the repair templates. Thus, in SETX-deficient cells, R-loops would accumulate on the BIR templates, causing TRC of DNA synthesis of BIR invading strands with active transcription, thereby inducing BIR template switching (Fig 7B). Therefore, SETX plays a critical role in the fidelity of BIR by reducing template switching, particularly at DSBs with active transcription. Although our study focuses on deDSBs, we speculate that on broken forks, if BIR templates are transcriptionally active, SETX would also be involved in suppressing template switching.

Structural variants (SVs) and copy number variants (CNVs) are abundantly observed in cancer genomes. Among these variants, the mechanisms of replication-associated CGR, often referred to as a copy-and-paste process (Li *et al*, 2020), are least understood. In the study of genomic disorders, such as Pelizaeus-Merzbacher disease (PMD), CGRs were identified with copy number increase with microhomologies present at the rearrangement junctions (Beck *et al*, 2015; Lee *et al*, 2007), and it has been proposed that microhomology-mediated BIR (MMBIR) is likely the underlying mechanism based on the rearrangement features (Hastings *et al*, 2009a; Hastings *et al*, 2009b). More recent analysis of cancer genomes has also uncovered CGRs with MMBIR features (Cortes-Ciriano *et al*, 2020; Li *et al.*, 2020; Osia *et al*, 2021). In a yeast study, local templated switching using microhomology sequences is observed when BIR is disrupted (Sakofsky *et al*, 2015). In this study, we showed that in mammalian cells, R-loop accumulation at BIR repair templates, could drastically induce template switching during BIR not only locally but also to other genome sites, resulting in genomic instability with MMBIR features. R-loop formation is widespread, occupying 5-10% of our genome under normal conditions, and our study indicates that BIR can be actively used at deDSBs

when R-loops are accumulated there. In addition, under replication stress, BIR is expected to be frequently used at seDSBs upon fork breakage. We therefore propose that BIR-mediated repair at R-loop-associated DSBs, including both deDSBs and seDSBs, could be a significant cause of MMBIR due to the high level of microhomology-mediated template switching, thereby being a significant contributor to replication-associated CGRs. Consequently, this process could be a major contributor to replication-associated CGRs.

SETX and cancer connection

The critical role of SETX in R-loop homeostasis and the preservation of genome stability suggests its potential involvement in tumor suppression (Gatti *et al.*, 2023). SETX gene is frequently mutated in cancers, and its expression is often downregulated in a variety of cancers, akin to other tumor suppressor genes (Rhodes *et al*, 2007). The newly identified role of SETX in suppressing mutagenic BIR and preventing template switching during BIR in this study reveals an unrecognized aspect of SETX in maintaining genome stability and provides new insights into the connection of SETX deficiency with genome instability and tumorigenesis. Moreover, we uncovered a pathway shift of HR (STGC) to utilizing the BIR mechanism at deDSBs in the transcriptionally active regions and demonstrated synthetic lethal interactions of SETX with PIF1 and RAD52. The pronounced reliance of SETX-deficient cells on PIF1 and RAD52 for cell viability lays a groundwork for establishing new treatment strategies through inhibiting PIF1 and RAD52 activity to selectively eradicate cancers with compromised SETX function, while preserving viability of normal cells.

Materials and Methods

Cell cultures

U2OS (ATCC), 293T (ATCC), *PIF1*-KO (Li *et al.*, 2021b), *RAD52*-KO (Liu *et al*, 2023) cells were cultured in DMEM media supplemented with 10% fetal bovine serum (FBS) and 1% penicillin/streptomycin at 37°C, 5% CO2.

Plasmid construction

The N-terminal Flag-tagged WT and helicase-dead (P-loopΔ) SETX-expressing plasmids are gifts from Dr. Craig Bennett (Bennett *et al.*, 2020). Their coding sequences were further cloned into pCDH-CMV-MCS-EF1-puro lentiviral vector (System Biosciences). The C-terminal V5-tagged WT RNASEH1 and D210N mutant plasmids are gifts from Dr. Xiangdong Fu (Chen *et al*, 2019). Their coding sequences were cloned into pCDH-CMV-MCS-EF1-puro lentiviral vector (System Biosciences). The 3xFlag-tagged D210N mutant used for chromatin immunoprecipitation (ChIP) was constructed by replacing the V5 tag with 3xFlag tag at C-terminal.

Generation of knock out (KO) cell line by CRISPR

Two sgRNAs sequences targeting coding sequence of specific genes were cloned into sgRNA/Cas9-mCherry vector derived from pSpCas9(BB)-2A-Puro (PX459) V2.0 vector (Addgene #62988). Two plasmids were transfected together into target cell lines using standard PEI protocol. Two days later, transfected cells were sorted for mCherry-positive events and plated for single clones. These single clones were screened with PCR or western blotting.

sgRNA sequences for *SETX*-KO:

aggctaaatccgttgatcac and TGTTGAAGCACTTTGTCGGA

sgRNA sequences for *XPF*-KO:

GGGCTAGTAGTGTGCGCCCG and GCTGGTGCTCAACACGCAGC

sgRNA sequences for *XPG*-KO:

acgtagccagcactaatgag and acctgggctcccgaatggaa

shRNA interference

Oligoes containing shRNA target sequences were cloned into pLKO.1-blast lentiviral vector (Addgene #26655). shRNA sequences used in this study are listed below.

SETXsh CGGCAGAAGGATTGTGTTATT

MRE11sh GATGAGAACTCTTGGTTTATT

CTIPsh GAGCAGACCTTTCTCAGTATA

BLMsh GAGCACATCTGTAAATTAATT

DNA2sh AGTTTGTGATGGGCAATATTT

EXO1sh ACTCGGATCTCCTAGCTTTTG

XPFsh AAGACGAGCTCACGAGTATTC

PIF1sh GAAGACAGGTGCTCCGGAAGC

PCNAsh GTGGAGAACTTGGAAATGGAA

Knockdown efficiency of individual shRNA was confirmed by Western blotting of whole-cell lysate or RT-qPCR with primers listed below.

EXO1_quanti_F TCGGATCTCCTAGCTTTTGGCTG

EXO1_quanti_R AGCTGTCTGCACATTCCTAGCC

DNA2_quanti_F GATTTCTGGCACCAGCATAGCC

DNA2_quanti_R ACACCTCATGGAGAACCGTACC

CTIP_quanti_F TGGCAGACAGTTTCTCCCAAGC

CTIP_quanti_R GGCTCCACAAACGCTTTCTGCT

PIF1_quanti_F CATCCACAAGAGCCAAGGCAT

PIF1_quanti_R GGTGGCATAGAAGTGCAGCA

BLM_quanti_F GGTGATAAGACTGACTCAGAAGC

BLM_quanti_R AACGTGCCAAGAGCTTCCTCTC

GAPDH_quanti_F GTCTCCTCTGACTTCAACAGCG

GAPDH_quanti_R ACCACCCTGTTGCTGTAGCCAA

RAD52_quanti_F GCCCAGAATACATAAGTAGCCGC

RAD52_quanti_R CCACATTCTGCTGCGTGATGGA

Colony formation assay

Colony formation assay was carried out to examine the potential synthetic lethality effect between SETX and other tested genes. Cells were infected with lentivirus to knock down indicated genes. Three days after infection, cells were resuspended and counted. For each condition, 5000 cells were plated on 10cm

plate. Two weeks later, plates with growing colonies were stained with 0.5% crystal violet in 20% methanol.

Western blotting

Cells cultured in 6-well plate were lysed in RIPA buffer (50 mM Tris–HCl, pH 8.0, 150 mM NaCl, 5 mM EDTA, 1% NP-40, 0.5% sodium deoxycholate, and 0.1% SDS). Fresh lysates were supplemented with eqaul amount of 2X loading buffer (100 mM Tris–Cl, pH 6.8, 4% SDS, 0.2% bromophenol blue, 20% glycerol, 200 mM DTT) and then boiled at 95°C for 5 min. Next, sampels were separated on 6–15% SDS–PAGE and proteins were transferred to nitrocellulose membrane (1620115, Bio-Rad) using the Trans-Blot Turbo Transfer System from Bio-Rad. Antibodies used were followed: SETX (NB100-57542, Novus Biologicals), KU70 (sc-17789, Santa Cruz Biotechnology), FLAG (F1804, Sigma-Aldrich), V5 (R96025, Invitrogen), XPF (sc-136153, Santa Cruz Biotechnology), RPA32 (Ser4/Ser8) (A300-245A, Bethyl Laboratories), γH2AX (2577, Cell Signaling Technology), PCNA (SC-56, Santa Cruz), GAPDH (AC002, ABclonal).

Immunostaining

Cells were seeded on coverslips in 6-well plate and cultured overnight in incubator. The next day, cells were first pre-extracted with 0.5% Trion X-100 in cold PBS for 5mins, then fixed with 1% formaldehyde for 10 mins at room temperature. Fixed cells were blocked with 5% milk in PBS for 30 mins and then incubated overnight with indicated primary antibodies diluted in PBS at 4°C. The next day, cells were washed with PBS for three times and further incubated with secondary antibody and DAPI. Finally, slides were sealed with mounting media (P36930, Invitrogen) to prevent quenching. Images were taken on Nikon ECLIPSE Ni-L microscope. Antibodies used were as followed: FLAG (F1804, Sigma-Aldrich), S9.6 (ENH001, Kerafast), γH2AX (2577, Cell Signaling Technology), RAD52 (sc-365341, Santa Cruz Biotechnology), XPF (sc-136153, Santa Cruz Biotechnology).

In situ proximity ligation assay (PLA)

Cells were seeded on coverslips in 6-well plate and cultured overnight in incubator. The next day, cells were treated with 4 Gy IR. Two hours later, cells were fixed and blocked the same way as immunostaining and then incubated with primary antibody overnight at 4°C. The next day, PLA was performed using the Duolink PLA kit (DUO92001 and DUO92005, Sigma-Aldrich) following the

manufacturer's protocol. Finally, slides were sealed with mounting media (P36930, Invitrogen) to prevent quenching. Images were taken on Nikon ECLIPSE Ni-L microscope. Primary antibodies used were as followed: FLAG (F1804, Sigma-Aldrich), PCNA (SC-56, Santa Cruz), γH2AX (07164, Upstate).

Chromatin immunoprecipitation (ChIP)

Cells growing on 10 cm plate were fixed with 1% formaldehyde for 10 min at room temperature and glycine was added to the final concentration of 0.125 M. Cells were scraped from the plate and lysed with 0.5% NP-40 buffer (10 mM Tris-HCl, 10 mM NaCl, 0.5% NP-40, freshly added Roche cOmplete protease inhibitor cocktail) for 15mins at 4°C. Whole lysates were sonicated with Bioruptor for 15 cycles (30s on/30s off) and then centrifuged to remove debris. Supernatent was collected and incubated with agarose beads conjugated with FLAG antibody (A2220, Millipore Sigma) for 4 hours at 4°C. After IP, beads were washed 3 times with 0.5% NP-40 buffer and once with TE buffer. Finally, beads was incubated in elution buffer (10 mM Tris-HCl, 1.0% SDS, 1.0 mM EDTA) overnight at 65°C to reverse the crosslinking. The next day, IP products and input were subjected to DNA extraction using phenol-chloroform. Recovered DNA was checked by qPCR to calculate the relative enrichement of target protein on specific locus. Primers used for ChIP were listed below.

At I-SceI-induced DSB end:

ChIP_L1F GAATCCATCTTGCTCCAACACCCC

ChIP_L1R CACAAACACAACTCCTCCGCGC

At repair template near CMV promoter:

ChIP_L5F CCCTGAAGTTCATCTGCACCACCG

ChIP_L5R cgagacttacCTGGACGTAGCCTTC

End resection quantification assay

The end resection assay in reporter cells was concepted from publications of Dr. Tanya Paull's lab (Zhou *et al.*, 2014) and modified according to our BIR reporter sequence. BIR reporter cells were infected with lentivirus expressing I-SceI to induce DSBs. Two days after infection, cells were harvested for genomic DNA extraction using Puregene Kits from QIAGEN. 1 ug genomic DNA was digested separately with NEB restriction enzyme BsiHKAI (left DSB end), ApoI (right DSB end) or SacII (mock) overnight. Restriction enzyme digested genomic DNA was used as template for qPCR with indicated primer listed

below.

L1:

End-Resection_L1F GCTCCAACACCCCAACATCTTCGAC

End-Resection_L1R CGGTACTTCGTCCACAAACACAACTCC

L3:

End-Resection_L3F GGTGAACTTCAAGATCCGCCACAAC

End-Resection_L3R CAGCTCGTCCATGCCGAGAG

R1:

End-Resection_R1F gaactagtggatcCCCTACCGTTCG

End-Resection_R1R ggtggatgtggaatgtgtgcgagg

R3:

End-Resection_R3F CGAGATCAGCAGCCTCTGTTCCACA

End-Resection_R3R CTGTCACCAATCCTGTCCCTAGTGCA

Laser microirradiation and live-cell imaging

EGFP-tagged protein was expressed by lentiviral vector in WT and *SETX*-KO U2OS cells. Laser microirradiation was applied to cells as previously described (Truong *et al*, 2013), which was performed using a Femto-second pulsed laser (780nm) with images recorded by a Zeiss Axiovert fluorescence microscope for live cell imaging in time series (Laboratory of Dr. Linda Shi, UCSD, CA).

LAM-HTGTS assay

This assay was adopted from a previous publication (Hu *et al.*, 2016) and modified to fit our BIR reporter system. EGFP-BIR-5085 reporter cells were infected with lentivirus expressing I-SceI to induce DSBs. Five days after infection, EGFP-positive cells were collected by FACS sorting and plated for single clones. Two weeks later, single clones were picked out and cultured in 6-well plate. When cells were confluent enough, genomic DNA was extracted with Puregene Kits from QIAGEN for each single clone. Equal amount of genomic DNA from indicated number of single clones was mixed together, and 500 ng mixed genomic DNA was used as template for LAM PCR, where biotin-labeled primer (Bio-R1) was supplemented together with 2x NEB Next Ultra II Q5 Master Mix (M0544L, NEB). LAM products were purified with Streptavidin C1 dynabeads (65001, Thermo Scientific). A customized linker (rand10_3Tr3) was added to the 3' end of on-bead LAM products using T4 RNA ligase I (M0204S, NEB). Nested PCR

was performed using indicated primer set (3Tr3-Adaptor_R and JM_F) with the ligated on-bead LAM products as templates. Products of nested PCR were further amplified using the Illumina indexing primer set (i501-508, i701-712). Final PCR products were sent for 1x100bp deep sequencing. CD-HIT (Fu *et al*, 2012) was used to cluster the sequencing results. Recovered sequences of each cluster were checked for translocations.

Sequences of oligoes used for PCR analysis and LAM-HTGTS assay are listed below.

PCR analysis:

F1 GGCATGGACGAGCTGTACAAGTAA

R1 gGTAGAATTTCGAggtcgaGGATC

LAM-HTGTS:

Bio-R1 /5Biosg/GAGGATCTGGGCTAGCCCTGATCAATAAC

rand10_3Tr3/5Phos/NNNNNNNNNNAGATCGGAAGAGCACACGTCTG/3SpC3/

JM_F CTTTCCCTACACGACGCTCTTCCGATCTGCTATACGAACGGTAGGGgatcc

3Tr3-Adaptor_R GTGACTGGAGTTCAGACGTGTGCTCTTCCGATCT

Statistical analysis

Student's t-test was run in two-tailed non-paired mode to examine the significance of differences between samples. In all experiments, error bars show standard deviation (SD) of at least three independent experiments. The P value is labeled as * $P < 0.05$, ** $P < 0.01$, *** $P < 0.001$, **** $P < 0.0001$, and ns (not significant) $P > 0.05$.

Acknowledgement

We would like thank Dr. Craig Bennett (University of Lincoln, UK) for providing the cDNA of WT and helicase-dead (P-loopΔ) mutant SETX, Dr. Xiangdong Fu (UCSD) for providing the WT and D210N mutant of RNASEH1 constructs. Plasmids pLKO.1-blast vector (26655) and pSpCas9(BB)-2A-Puro (PX459) V2.0 (62988) are from Addgene. This study is funded by NIH grants CA244912, GM141868 and CA187052 to X.W.

Author contributions

T.W. designed and performed experiments and analyzed the data; Y.L. and L.S. conducted some experiments. X.W. is responsible for the overall project's planning and experimental design. T.W. and X.W. wrote the manuscript.

Disclosure and competing interests statement

The authors declare no competing financial interests.

Reference

Alfano L, Caporaso A, Altieri A, Dell'Aquila M, Landi C, Bini L, Pentimalli F, Giordano A (2019) Depletion of the RNA binding protein HNRNPD impairs homologous recombination by inhibiting DNA-end resection and inducing R-loop accumulation. *Nucleic Acids Res* 47: 4068-4085

Alzu A, Bermejo R, Begnis M, Lucca C, Piccini D, Carotenuto W, Saponaro M, Brambati A, Cocito A, Foiani M *et al* (2012) Senataxin associates with replication forks to protect fork integrity across RNA-polymerase-II-transcribed genes. *Cell* 151: 835-846

Anand R, Jasrotia A, Bundschuh D, Howard SM, Ranjha L, Stucki M, Cejka P (2019) NBS1 promotes the endonuclease activity of the MRE11-RAD50 complex by sensing CtIP phosphorylation. *EMBO J* 38

Anand R, Ranjha L, Cannavo E, Cejka P (2016) Phosphorylated CtIP Functions as a Co-factor of the MRE11-RAD50-NBS1 Endonuclease in DNA End Resection. *Mol Cell* 64: 940-950

Anand RP, Tsaponina O, Greenwell PW, Lee CS, Du W, Petes TD, Haber JE (2014) Chromosome rearrangements via template switching between diverged repeated sequences. *Genes Dev* 28: 2394-2406

Beck CR, Carvalho CM, Banser L, Gambin T, Stubbolo D, Yuan B, Sperle K, McCahan SM, Henneke M, Seeman P *et al* (2015) Complex genomic rearrangements at the PLP1 locus include triplication and quadruplication. *PLoS Genet* 11: e1005050

Bennett CL, Sopher BL, La Spada AR (2020) Tight expression regulation of senataxin, linked to motor neuron disease and ataxia, is required to avert cell-cycle block and nucleolus disassembly. *Heliyon* 6: e04165

Bhowmick R, Hickson ID, Liu Y (2023) Completing genome replication outside of S phase. *Mol Cell* 83: 3596-3607

Brickner JR, Garzon JL, Cimprich KA (2022) Walking a tightrope: The complex balancing act of R-loops in genome stability. *Mol Cell* 82: 2267-2297

Buzovetsky O, Kwon Y, Pham NT, Kim C, Ira G, Sung P, Xiong Y (2017) Role of the Pif1-PCNA Complex in Pol δ-Dependent Strand Displacement DNA Synthesis and Break-Induced Replication. *Cell Reports* 21: 1707-1714

Cannavo E, Cejka P (2014) Sae2 promotes dsDNA endonuclease activity within Mre11-Rad50-Xrs2 to resect DNA breaks. *Nature* 514: 122-125

Ceccaldi R, Rondinelli B, D'Andrea AD (2016) Repair Pathway Choices and Consequences at the Double-Strand Break. *Trends Cell Biol* 26: 52-64

Cejka P, Symington LS (2021) DNA End Resection: Mechanism and Control. *Annu Rev Genet* 55: 285-307

Chang EY, Tsai S, Aristizabal MJ, Wells JP, Coulombe Y, Busatto FF, Chan YA, Kumar A, Dan Zhu Y, Wang AY *et al* (2019) MRE11-RAD50-NBS1 promotes Fanconi Anemia R-loop suppression at transcription-replication conflicts. *Nat Commun* 10: 4265

Chen JY, Zhang X, Fu XD, Chen L (2019) R-ChIP for genome-wide mapping of R-loops by using catalytically inactive RNASEH1. *Nat Protoc* 14: 1661-1685

Chen L, Chen JY, Zhang X, Gu Y, Xiao R, Shao C, Tang P, Qian H, Luo D, Li H *et al* (2017) R-ChIP Using Inactive RNase H Reveals Dynamic Coupling of R-loops with Transcriptional Pausing at Gene Promoters. *Mol Cell* 68: 745-757 e745

Chen YZ, Bennett CL, Huynh HM, Blair IP, Puls I, Irobi J, Dierick I, Abel A, Kennerson ML, Rabin BA *et al* (2004) DNA/RNA helicase gene mutations in a form of juvenile amyotrophic lateral sclerosis (ALS4). *Am J Hum Genet* 74: 1128-1135

Chen YZ, Hashemi SH, Anderson SK, Huang Y, Moreira MC, Lynch DR, Glass IA, Chance PF, Bennett CL (2006) Senataxin, the yeast Sen1p orthologue: characterization of a unique protein in which

recessive mutations cause ataxia and dominant mutations cause motor neuron disease. *Neurobiol Dis* 23: 97-108
Cohen S, Guenole A, Lazar I, Marnef A, Clouaire T, Vernekar DV, Puget N, Rocher V, Arnould C, Aguirrebengoa M *et al* (2022) A POLD3/BLM dependent pathway handles DSBs in transcribed chromatin upon excessive RNA:DNA hybrid accumulation. *Nat Commun* 13: 2012
Cohen S, Puget N, Lin YL, Clouaire T, Aguirrebengoa M, Rocher V, Pasero P, Canitrot Y, Legube G (2018) Senataxin resolves RNA:DNA hybrids forming at DNA double-strand breaks to prevent translocations. *Nat Commun* 9: 533
Cortes-Ciriano I, Lee JJ, Xi R, Jain D, Jung YL, Yang L, Gordenin D, Klimczak LJ, Zhang CZ, Pellman DS *et al* (2020) Comprehensive analysis of chromothripsis in 2,658 human cancers using whole-genome sequencing. *Nat Genet* 52: 331-341
Crossley MP, Song C, Bocek MJ, Choi JH, Kousorous J, Sathirachinda A, Lin C, Brickner JR, Bai G, Lans H *et al* (2023) R-loop-derived cytoplasmic RNA-DNA hybrids activate an immune response. *Nature* 613: 187-194
D'Alessandro G, Whelan DR, Howard SM, Vitelli V, Renaudin X, Adamowicz M, Iannelli F, Jones-Weinert CW, Lee M, Matti V *et al* (2018) BRCA2 controls DNA:RNA hybrid level at DSBs by mediating RNase H2 recruitment. *Nat Commun* 9: 5376
Daley JM, Tomimatsu N, Hooks G, Wang W, Miller AS, Xue X, Nguyen KA, Kaur H, Williamson E, Mukherjee B *et al* (2020) Specificity of end resection pathways for double-strand break regions containing ribonucleotides and base lesions. *Nat Commun* 11: 3088
Deem A, Keszthelyi A, Blackgrove T, Vayl A, Coffey B, Mathur R, Chabes A, Malkova A (2011) Break-induced replication is highly inaccurate. *PLoS Biol* 9: e1000594
Deshpande RA, Lee JH, Arora S, Paull TT (2016) Nbs1 Converts the Human Mre11/Rad50 Nuclease Complex into an Endo/Exonuclease Machine Specific for Protein-DNA Adducts. *Mol Cell* 64: 593-606
Domingo-Prim J, Endara-Coll M, Bonath F, Jimeno S, Prados-Carvajal R, Friedlander MR, Huertas P, Visa N (2019) EXOSC10 is required for RPA assembly and controlled DNA end resection at DNA double-strand breaks. *Nat Commun* 10: 2135
Fu L, Niu B, Zhu Z, Wu S, Li W (2012) CD-HIT: accelerated for clustering the next-generation sequencing data. *Bioinformatics* 28: 3150-3152
Gao M, Wei W, Li MM, Wu YS, Ba Z, Jin KX, Li MM, Liao YQ, Adhikari S, Chong Z *et al* (2014) Ago2 facilitates Rad51 recruitment and DNA double-strand break repair by homologous recombination. *Cell Res* 24: 532-541
Garcia-Muse T, Aguilera A (2019) R Loops: From Physiological to Pathological Roles. *Cell* 179: 604-618
Gatti V, De Domenico S, Melino G, Peschiaroli A (2023) Senataxin and R-loops homeostasis: multifaced implications in carcinogenesis. *Cell Death Discov* 9: 145
Giannini M, Porrua O (2024) Senataxin: A key actor in RNA metabolism, genome integrity and neurodegeneration. *Biochimie* 217: 10-19
Glover TW, Wilson TE, Arlt MF (2017) Fragile sites in cancer: more than meets the eye. *Nat Rev Cancer* 17: 489-501
Groh M, Albulescu LO, Cristini A, Gromak N (2017) Senataxin: Genome Guardian at the Interface of Transcription and Neurodegeneration. *J Mol Biol* 429: 3181-3195
Hastings PJ, Ira G, Lupski JR (2009a) A microhomology-mediated break-induced replication model for the origin of human copy number variation. *PLoS Genet* 5: e1000327
Hastings PJ, Lupski JR, Rosenberg SM, Ira G (2009b) Mechanisms of change in gene copy number. *Nat Rev Genet* 10: 551-564

Hatchi E, Skourti-Stathaki K, Ventz S, Pinello L, Yen A, Kamieniarz-Gdula K, Dimitrov S, Pathania S, McKinney KM, Eaton ML *et al* (2015) BRCA1 recruitment to transcriptional pause sites is required for R-loop-driven DNA damage repair. *Mol Cell* 57: 636-647
Helmrich A, Ballarino M, Tora L (2011) Collisions between replication and transcription complexes cause common fragile site instability at the longest human genes. *Mol Cell* 44: 966-977
Hu J, Meyers RM, Dong J, Panchakshari RA, Alt FW, Frock RL (2016) Detecting DNA double-stranded breaks in mammalian genomes by linear amplification-mediated high-throughput genome-wide translocation sequencing. *Nat Protoc* 11: 853-871
Hustedt N, Durocher D (2016) The control of DNA repair by the cell cycle. *Nat Cell Biol* 19: 1-9
Jackson SP, Bartek J (2009) The DNA-damage response in human biology and disease. *Nature* 461: 1071-1078
Jain S, Sugawara N, Lydeard J, Vaze M, Tanguy Le Gac N, Haber JE (2009) A recombination execution checkpoint regulates the choice of homologous recombination pathway during DNA double-strand break repair. *Genes Dev* 23: 291-303
Khanna KK, Jackson SP (2001) DNA double-strand breaks- signaling, repair and the cancer connection. *Nature Genet* 27: 247–254
Kramara J, Osia B, Malkova A (2018) Break-Induced Replication: The Where, The Why, and The How. *Trends Genet* 34: 518-531
Lee JA, Carvalho CM, Lupski JR (2007) A DNA replication mechanism for generating nonrecurrent rearrangements associated with genomic disorders. *Cell* 131: 1235-1247
Li L, Germain DR, Poon HY, Hildebrandt MR, Monckton EA, McDonald D, Hendzel MJ, Godbout R (2016) DEAD Box 1 Facilitates Removal of RNA and Homologous Recombination at DNA Double-Strand Breaks. *Mol Cell Biol* 36: 2794-2810
Li S, Wang H, Jehi S, Li J, Liu S, Wang Z, Truong L, Chiba T, Wang Z, Wu X (2021a) PIF1 helicase promotes break-induced replication in mammalian cells. *EMBO J*: e104509
Li S, Wang H, Jehi S, Li J, Liu S, Wang Z, Truong L, Chiba T, Wang Z, Wu X (2021b) PIF1 helicase promotes break-induced replication in mammalian cells. *EMBO J* 40: e104509
Li S, Wu X (2020) Common fragile sites: protection and repair. *Cell Biosci* 10: 29
Li Y, Roberts ND, Wala JA, Shapira O, Schumacher SE, Kumar K, Khurana E, Waszak S, Korbel JO, Haber JE *et al* (2020) Patterns of somatic structural variation in human cancer genomes. *Nature* 578: 112-121
Liaw H, Lee D, Myung K (2011) DNA-PK-dependent RPA2 hyperphosphorylation facilitates DNA repair and suppresses sister chromatid exchange. *PLoS One* 6: e21424
Liu L, Malkova A (2022) Break-induced replication: unraveling each step. *Trends Genet* 38: 752-765
Liu L, Yan Z, Osia BA, Twarowski J, Sun L, Kramara J, Lee RS, Kumar S, Elango R, Li H *et al* (2021) Tracking break-induced replication shows that it stalls at roadblocks. *Nature*
Liu S, Wang Z, Shah SB, Chang CY, Ai M, Nguyen T, Xiang R, Wu X (2023) DNA repair protein RAD52 is required for protecting G-quadruplexes in mammalian cells. *J Biol Chem* 299: 102770
Makharashvili N, Arora S, Yin Y, Fu Q, Wen X, Lee JH, Kao CH, Leung JW, Miller KM, Paull TT (2018) Sae2/CtIP prevents R-loop accumulation in eukaryotic cells. *Elife* 7
Marnef A, Legube G (2021) R-loops as Janus-faced modulators of DNA repair. *Nat Cell Biol* 23: 305-313
Matsui M, Sakasai R, Abe M, Kimura Y, Kajita S, Torii W, Katsuki Y, Ishiai M, Iwabuchi K, Takata M *et al* (2020) USP42 enhances homologous recombination repair by promoting R-loop resolution with a DNA-RNA helicase DHX9. *Oncogenesis* 9: 60
Mehta A, Beach A, Haber JE (2017) Homology Requirements and Competition between Gene

Conversion and Break-Induced Replication during Double-Strand Break Repair. *Mol Cell* 65: 515-526 e513
Michelini F, Pitchiaya S, Vitelli V, Sharma S, Gioia U, Pessina F, Cabrini M, Wang Y, Capozzo I, Iannelli F *et al* (2017) Damage-induced lncRNAs control the DNA damage response through interaction with DDRNAs at individual double-strand breaks. *Nat Cell Biol* 19: 1400-1411
Moreira MC, Klur S, Watanabe M, Nemeth AH, Le Ber I, Moniz JC, Tranchant C, Aubourg P, Tazir M, Schols L *et al* (2004) Senataxin, the ortholog of a yeast RNA helicase, is mutant in ataxia-ocular apraxia 2. *Nat Genet* 36: 225-227
Motycka TA, Bessho T, Post SM, Sung P, Tomkinson AE (2004) Physical and functional interaction between the XPF/ERCC1 endonuclease and hRad52. *J Biol Chem* 279: 13634-13639
Naim V, Wilhelm T, Debatisse M, Rosselli F (2013) ERCC1 and MUS81-EME1 promote sister chromatid separation by processing late replication intermediates at common fragile sites during mitosis. *Nat Cell Biol* 15: 1008-1015
Niehrs C, Luke B (2020) Regulatory R-loops as facilitators of gene expression and genome stability. *Nat Rev Mol Cell Biol* 21: 167-178
Ohle C, Tesorero R, Schermann G, Dobrev N, Sinning I, Fischer T (2016) Transient RNA-DNA Hybrids Are Required for Efficient Double-Strand Break Repair. *Cell* 167: 1001-1013 e1007
Osia B, Alsulaiman T, Jackson T, Kramara J, Oliveira S, Malkova A (2021) Cancer cells are highly susceptible to accumulation of templated insertions linked to MMBIR. *Nucleic Acids Res* 49: 8714-8731
Ozeri-Galai E, Bester AC, Kerem B (2012) The complex basis underlying common fragile site instability in cancer. *Trends Genet* 28: 295-302
Pardo B, Aguilera A (2012) Complex chromosomal rearrangements mediated by break-induced replication involve structure-selective endonucleases. *PLoS Genet* 8: e1002979
Petermann E, Lan L, Zou L (2022) Sources, resolution and physiological relevance of R-loops and RNA-DNA hybrids. *Nat Rev Mol Cell Biol* 23: 521-540
Pham N, Yan Z, Yu Y, Faria Afreen M, Malkova A, Haber JE, Ira G (2021) Mechanisms restraining break-induced replication at two-ended DNA double-strand breaks. *EMBO J* 40: e104847
Quinet A, Lemacon D, Vindigni A (2017) Replication Fork Reversal: Players and Guardians. *Mol Cell* 68: 830-833
Rawal CC, Zardoni L, Di Terlizzi M, Galati E, Brambati A, Lazzaro F, Liberi G, Pellicioli A (2020) Senataxin Ortholog Sen1 Limits DNA:RNA Hybrid Accumulation at DNA Double-Strand Breaks to Control End Resection and Repair Fidelity. *Cell reports* 31: 107603
Rhodes DR, Kalyana-Sundaram S, Mahavisno V, Varambally R, Yu J, Briggs BB, Barrette TR, Anstet MJ, Kincead-Beal C, Kulkarni P *et al* (2007) Oncomine 3.0: genes, pathways, and networks in a collection of 18,000 cancer gene expression profiles. *Neoplasia* 9: 166-180
Richard P, Feng S, Manley JL (2013) A SUMO-dependent interaction between Senataxin and the exosome, disrupted in the neurodegenerative disease AOA2, targets the exosome to sites of transcription-induced DNA damage. *Genes Dev* 27: 2227-2232
Sakofsky CJ, Ayyar S, Deem AK, Chung WH, Ira G, Malkova A (2015) Translesion Polymerases Drive Microhomology-Mediated Break-Induced Replication Leading to Complex Chromosomal Rearrangements. *Mol Cell* 60: 860-872
Sakofsky CJ, Malkova A (2017) Break induced replication in eukaryotes: mechanisms, functions, and consequences. *Crit Rev Biochem Mol Biol* 52: 395-413
Sessa G, Gomez-Gonzalez B, Silva S, Perez-Calero C, Beaurepere R, Barroso S, Martineau S, Martin C, Ehlen A, Martinez JS *et al* (2021) BRCA2 promotes DNA-RNA hybrid resolution by DDX5 helicase at DNA breaks to facilitate their repairdouble dagger. *EMBO J* 40: e106018

Shibata A, Moiani D, Arvai AS, Perry J, Harding SM, Genois MM, Maity R, van Rossum-Fikkert S, Kertokalio A, Romoli F *et al* (2014) DNA double-strand break repair pathway choice is directed by distinct MRE11 nuclease activities. *Mol Cell* 53: 7-18
Smith CE, Llorente B, Symington LS (2007) Template switching during break-induced replication. *Nature* 447: 102-105
Sobinoff AP, Pickett HA (2017) Alternative Lengthening of Telomeres: DNA Repair Pathways Converge. *Trends Genet* 33: 921-932
Sollier J, Stork CT, Garcia-Rubio ML, Paulsen RD, Aguilera A, Cimprich KA (2014) Transcription-coupled nucleotide excision repair factors promote R-loop-induced genome instability. *Mol Cell* 56: 777-785
Stork CT, Bocek M, Crossley MP, Sollier J, Sanz LA, Chedin F, Swigut T, Cimprich KA (2016) Co-transcriptional R-loops are the main cause of estrogen-induced DNA damage. *Elife* 5
Suraweera A, Lim Y, Woods R, Birrell GW, Nasim T, Becherel OJ, Lavin MF (2009) Functional role for senataxin, defective in ataxia oculomotor apraxia type 2, in transcriptional regulation. *Human molecular genetics* 18: 3384-3396
Tan J, Duan M, Yadav T, Phoon L, Wang X, Zhang JM, Zou L, Lan L (2020) An R-loop-initiated CSB-RAD52-POLD3 pathway suppresses ROS-induced telomeric DNA breaks. *Nucleic Acids Res* 48: 1285-1300
Tian M, Alt FW (2000) Transcription-induced cleavage of immunoglobulin switch regions by nucleotide excision repair nucleases in vitro. *J Biol Chem* 275: 24163-24172
Truong LN, Li Y, Shi LZ, Hwang PY, He J, Wang H, Razavian N, Berns MW, Wu X (2013) Microhomology-mediated End Joining and Homologous Recombination share the initial end resection step to repair DNA double-strand breaks in mammalian cells. *Proc Natl Acad Sci U S A* 110: 7720-7725
Ursic D, Chinchilla K, Finkel JS, Culbertson MR (2004) Multiple protein/protein and protein/RNA interactions suggest roles for yeast DNA/RNA helicase Sen1p in transcription, transcription-coupled DNA repair and RNA processing. *Nucleic Acids Res* 32: 2441-2452
Wilson MA, Kwon Y, Xu Y, Chung WH, Chi P, Niu H, Mayle R, Chen X, Malkova A, Sung P *et al* (2013) Pif1 helicase and Poldelta promote recombination-coupled DNA synthesis via bubble migration. *Nature* 502: 393-396
Wu X, Malkova A (2021) Break-induced replication mechanisms in yeast and mammals. *Curr Opin Genet Dev* 71: 163-170
Yasuhara T, Kato R, Hagiwara Y, Shiotani B, Yamauchi M, Nakada S, Shibata A, Miyagawa K (2018) Human Rad52 Promotes XPG-Mediated R-loop Processing to Initiate Transcription-Associated Homologous Recombination Repair. *Cell* 175: 558-570 e511
Ying S, Minocherhomji S, Chan KL, Palmai-Pallag T, Chu WK, Wass T, Mankouri HW, Liu Y, Hickson ID (2013) MUS81 promotes common fragile site expression. *Nat Cell Biol* 15: 1001-1007
Yu Z, Mersaoui SY, Guitton-Sert L, Coulombe Y, Song J, Masson JY, Richard S (2020) DDX5 resolves R-loops at DNA double-strand breaks to promote DNA repair and avoid chromosomal deletions. *NAR Cancer* 2: zcaa028
Yuce O, West SC (2013) Senataxin, defective in the neurodegenerative disorder ataxia with oculomotor apraxia 2, lies at the interface of transcription and the DNA damage response. *Mol Cell Biol* 33: 406-417
Zdravkovic A, Daley JM, Dutta A, Niwa T, Murayama Y, Kanamaru S, Ito K, Maki T, Argunhan B, Takahashi M *et al* (2021) A conserved Ctp1/CtIP C-terminal peptide stimulates Mre11 endonuclease activity. *Proc Natl Acad Sci U S A* 118
Zhao H, Hartono SR, de Vera KMF, Yu Z, Satchi K, Zhao T, Sciammas R, Sanz L, Chedin F, Barlow J

(2022) Senataxin and RNase H2 act redundantly to suppress genome instability during class switch recombination. *Elife* 11
Zhou Y, Caron P, Legube G, Paull TT (2014) Quantitation of DNA double-strand break resection intermediates in human cells. *Nucleic Acids Res* 42: e19

Figure Legends

Figure 1. SETX loss induces hyperrecombination for both HR and BIR in an R-loop-dependent manner.

A, B. Schematic drawing of EGFP-HR-5633 (A) and EGFP-BIR-5085 (B) reporters.

C, D. U2OS WT and *SETX*-KO EGFP-HR-5633 (C) and EGFP-BIR-5085 (D) reporter cells expressing SETX shRNA or vector, were infected with lentivirus expressing I-SceI to induce DSBs. The percentage of EGFP-positive cells was quantified by FACS analysis five days later (top). The efficiency of SETX knockdown or knockout were determined by Western blotting (bottom).

E. U2OS WT or *SETX*-KO EGFP-BIR-5085 reporter cells were infected with lentivirus expressing Flag-tagged intact SETX or mutated SETX, then infected with lentivirus expressing I-SceI to induce DSBs. The percentage of EGFP-positive cells was quantified by FACS analysis five days later (Left). The expression of Flag-SETX was determined by western blotting (Right).

F. U2OS WT and *SETX*-KO EGFP-BIR-5085 reporter cells were infected with lentivirus expressing V5-tagged RNASEH1. Control cells and RNASEH1-expressing cells were fixed and subjected to immunostaining with S9.6 antibody to quantify R-loop level.

G, H. EGFP-HR-5633 (G) or EGFP-BIR-5085 (H) reporter cells with or without V5-tagged RNASEH1 expression were infected with lentivirus expressing SETX shRNA or vector. Three days later, all cells were infected with lentivirus expressing I-SceI to induce DSBs. The percentage of EGFP-positive cells was quantified by FACS analysis five days later (Left). The expression level of SETX and RNASEH1-V5 was determined by western blotting (Right).

Figure 2. HR in SETX-deficient cells resembles BIR.

A. U2OS WT and *PIF1*-KO EGFP-BIR-5085 reporter cells were infected with SETX shRNA or vector. After three days, all cells were infected with I-SceI-expressing lentivirus to induce DSBs. The percentage of EGFP-positive cells was quantified by FACS analysis five days later.

B. U2OS WT and *SETX*-KO EGFP-HR-5633 reporter cells were infected with PIF1 shRNA or vector. After three days, all cells were infected with I-SceI-expressing lentivirus to induce DSBs. The percentage of EGFP-positive cells was quantified by FACS analysis five days later.

C. WT and *SETX*-KO U2OS cells were infected with PIF1-EGFP-expressing lentivirus. Cells with PIF1-EGFP expression were treated with 30 mW laser as marked by black lines to induce DNA damage. The formation of PIF1-EGFP strips was recorded at the indicated time points.

D. U2OS cells with or without V5-tagged RNASEH1 expression were infected with SETX shRNA or vector. Four days later, all cells were subjected to immunostaining using γ-H2AX antibody (left). Quantification of γ-H2AX foci is shown on the right.

E. U2OS cells were infected with vector, SETX shRNA, PIF1 shRNA, or both SETX and PIF1 shRNA. Cell lysates were collected four days after virus infection and checked with Western blotting.

F. U2OS cells were infected with vector, SETX shRNA, PIF1 shRNA, or both SETX and PIF1 shRNA. Three days after infection, cells were resuspended and counted. 5000 cells were seeded on plates and cultured for two weeks, then stained with crystal violet.

G. WT and *SETX*-KO U2OS cells were infected with lentivirus expressing Flag-tagged PIF1. Cells with Flag-PIF1 expression were treated with 4 Gy IR. Two hours later, the co-localization of Flag-PIF1 and γ-H2AX was analyzed by PLA.

H. WT and *SETX*-KO U2OS cells were treated with 4 Gy IR. Two hours later, the co-localization of PCNA and γ-H2AX was analyzed by PLA.

I. *SETX*-KO U2OS cells with Flag-PIF1 expression were infected with PCNA shRNA or vector. Three days later, cells were subjected to 4 Gy IR. Two hours after IR, the co-localization of Flag-Pif1 and γ-H2AX was analyzed by PLA.

Figure 3. SETX loss induces excessive end resection.

A. WT and *SETX*-KO U2OS cells were treated with 10 Gy IR. Cell lysates were collected at indicated time points and checked with western blotting.

B. Illustration of site-specific end resection assay in EGFP-BIR-5085 reporter. Cells are infected with I-SceI-expressing lentivirus to induce DSBs. After two days, genomic DNA (gDNA) is extracted and digested with indicated restriction enzyme (RE): BsiHKAI for the left DSB ends, ApoI for the right DSB ends, or SacII as mock for both ends. RE-resistant ssDNA is quantified by qPCR using primer sets around the RE recognition sites.

C. WT and *SETX*-KO U2OS cells were infected with lentivirus expressing RPA2-EGFP to make constant expression of RPA2-EGFP. Cells with RPA2-EGFP expression were treated with 30 mW laser marked in black lines to induce DNA damage. The formation of RPA2-EGFP strips was recorded at the indicated time points.

D. U2OS EGFP-BIR-5085 reporter cells with Flag-RNASEH1(D210N) expression were infected with SETX shRNA or vector. Four days later, cells were harvested for ChIP analysis.

E. U2OS EGFP-BIR-5085 reporter cells with or without RNASEH1-V5 expression were infected with SETX shRNA or vector. Three days after infection, cells were infected with I-SceI-expressing lentivirus to induce DSBs. Three days after the second infection, cells were harvested for gDNA for end resection assay.

F. WT and *SETX*-KO U2OS cells with or without RNASEH1-V5 expression were treated with 10 Gy IR. Cell lysates were collected one hour after IR and checked with western blotting.

Figure 4. SETX loss activates non-canonical resection pathway.

A, B, C. U2OS WT and *SETX*-KO EGFP-BIR-5085 reporter cells were infected with MRE11 shRNA, CtIP shRNA, or vector. Three days were given to allow shRNA expression to achieve effective knockdown of each gene. For BIR efficiency analysis (A), shRNA-treated cells were infected with I-SceI-expressing lentivirus to induce DSBs. The percentage of EGFP-positive cells was quantified by FACS analysis five days after I-SceI infection. For end resection assay (B), shRNA-treated cells were infected with I-SceI-expressing lentivirus to induce DSBs. Two days after I-SceI infection, cells were harvested for end resection assay. For the pRPA2 level (C), shRNA-treated cells were treated with 10 Gy IR. Cell lysates were collected one hour after IR and checked with western blotting.

D. U2OS WT and *SETX*-KO EGFP-BIR-5085 reporter cells were infected with XPF shRNA or vector. Three days later, cells were infected with I-SceI-expressing lentivirus to induce DSBs. Inhibitor PFM01 (100 uM) or DMSO was applied to cells together with I-SceI lentivirus. Two days after I-SceI infection, cells were harvested for end resection assay.

E. U2OS WT and *SETX*-KO EGFP-BIR-5085 reporter cells were infected with I-SceI to induce DSBs, simultaneously treated with DMSO or inhibitor PFM39 (100 uM). Two days after I-SceI infection, cells were harvested for end resection assay.

F, G. U2OS WT and *SETX*-KO EGFP-BIR-5085 reporter cells were infected with BLM shRNA, DNA2 shRNA, EXO1 shRNA, or vector. Three days later, cells were then infected with I-SceI-expressing lentivirus to induce DSBs for end resection assay (F), or treated with 10 Gy IR to check pRPA2 level (G).

Figure 5. R-loop accumulation activates RAD52-XPF to initiate end resection in SETX-deficient cells.

A, B. U2OS WT and SETX-KO EGFP-BIR-5085 reporter cells were infected with XPF shRNA or

vector. Three days after infection, cells were infected with I-SceI-expressing lentivirus to induce DSBs. The percentage of EGFP-positive cells was quantified by FACS analysis five days after I-SceI infection (A), and end resection assay was performed two days after I-SceI infection (B).

C, D. U2OS WT and *RAD52*-KO EGFP-BIR-5085 reporter cells were infected with SETX shRNA or vector. Three days after infection, cells were infected with I-SceI-expressing lentivirus to induce DSBs. The percentage of EGFP-positive cells was quantified by FACS analysis five days after I-SceI infection (C), and end resection assay was performed two days after I-SceI infection (D).

E. WT, *RAD52*-KO, and *XPF*-KO U2OS cells were infected with SETX shRNA or vector. Three days later, cells were treated with 10 Gy IR. Cell lysates were collected one hour after IR and checked with western blotting.

F. U2OS cells with or without RNASEH1-V5 expression were infected with SETX shRNA or vector. Three days later, cells were treated with 10 Gy IR. Cells were subjected to immunostaining with RAD52 antibody one hour after IR.

G. WT and *RAD52*-KO U2OS cells were infected with SETX shRNA or vector. Three days later, cells were treated with 10 Gy IR. Cells were subjected to immunostaining with XPF antibody one hour after IR.

H. WT, *RAD52*-KO, and *XPF*-KO U2OS cells were infected with SETX shRNA or vector. Three days after infection, cells were resuspended and counted. 5000 cells were seeded on plates and cultured for two weeks, then stained with crystal violet.

Figure 6. SETX deficiency promotes template switching during BIR in an R-loop-dependent manner.

A. Summary of template switching events identified from both PCR analysis and LAM-HTGTS. U2OS WT and *SETX*-KO EGFP-BIR-5085 reporter cells with or without RNASEH1-V5 expression were infected with I-SceI lentivirus to induce DSBs. Five days after infection, EGFP-positive cells were sorted as BIR-positive events. BIR repair products in these cells were analyzed by PCR or LAM-HTGTS (Fig S4A and S4B) to determine the occurrence of template switching or not. Template switching events are classified according to where the inserted sequences come from. If a template switching event only copies sequences inside of the BIR reporter, it is defined as “within reporter”. If a template switching event copies sequences outside of the BIR reporter in the surrounding regions on the same chromosome or even from other chromosomes, it will be regarded as “outside reporter”. If a template switching event

contains sequences from lentiviral plasmids that have been delivered to cells during experiments, it will be marked as "plasmid". The frequency of template switching was calculated as the number of total template switching events, including "within reporter", "outside reporter", and "plasmid", divided by the number of EGFP-positive clones.

B. Template switching events defined as "outside reporter" in A are displayed in Circos plot.

C. U2OS WT EGFP-BIR-5085 reporter cells with or without RNASEH1-V5 expression were infected with SETX shRNA. Three days after infection, cells were infected with I-SceI-expressing lentivirus to induce DSBs. Two days after the second infection, cells were harvested for site-specific ChIP-qPCR analysis to determine the R-loop level.

D. Examples of "within reporter" template switching events in U2OS WT and *SETX*-KO EGFP-BIR-5085 reporter cells summarized in A.

E. Summary of tract length data of recovered BIR repair products in U2OS WT and *SETX*-KO EGFP-BIR-5085 reporter cells with or without RNASEH1 overexpression. Red lines mark the median tract length in each group.

Figure 7. Model of BIR and associated template switching in SETX-deficient cells.

A. SETX deficiency causes more R-loop formation on DSB ends, which recruits RAD52, which in turn recruits XPF. Instead of MRE11, XPF generates nicks on the 5' strand. After nicking, MRE11 removes the remaining 5' strand towards DSB ends with its 3' to 5' exonuclease activity. Long-range resection proteins EXO1 and BLM/DNA2 digest 5' strand away from DSB ends.

B. SETX deficiency causes increased R-loop formation on the repair templates. After strand invasion, BIR DNA synthesis would encounter R-loops on the repair template, which could impair BIR fork progression and cause displacement of the synthesizing strand. Reassembly of collapsed BIR forks using templates at other genomic loci gives rise to template switching.

Fig 1

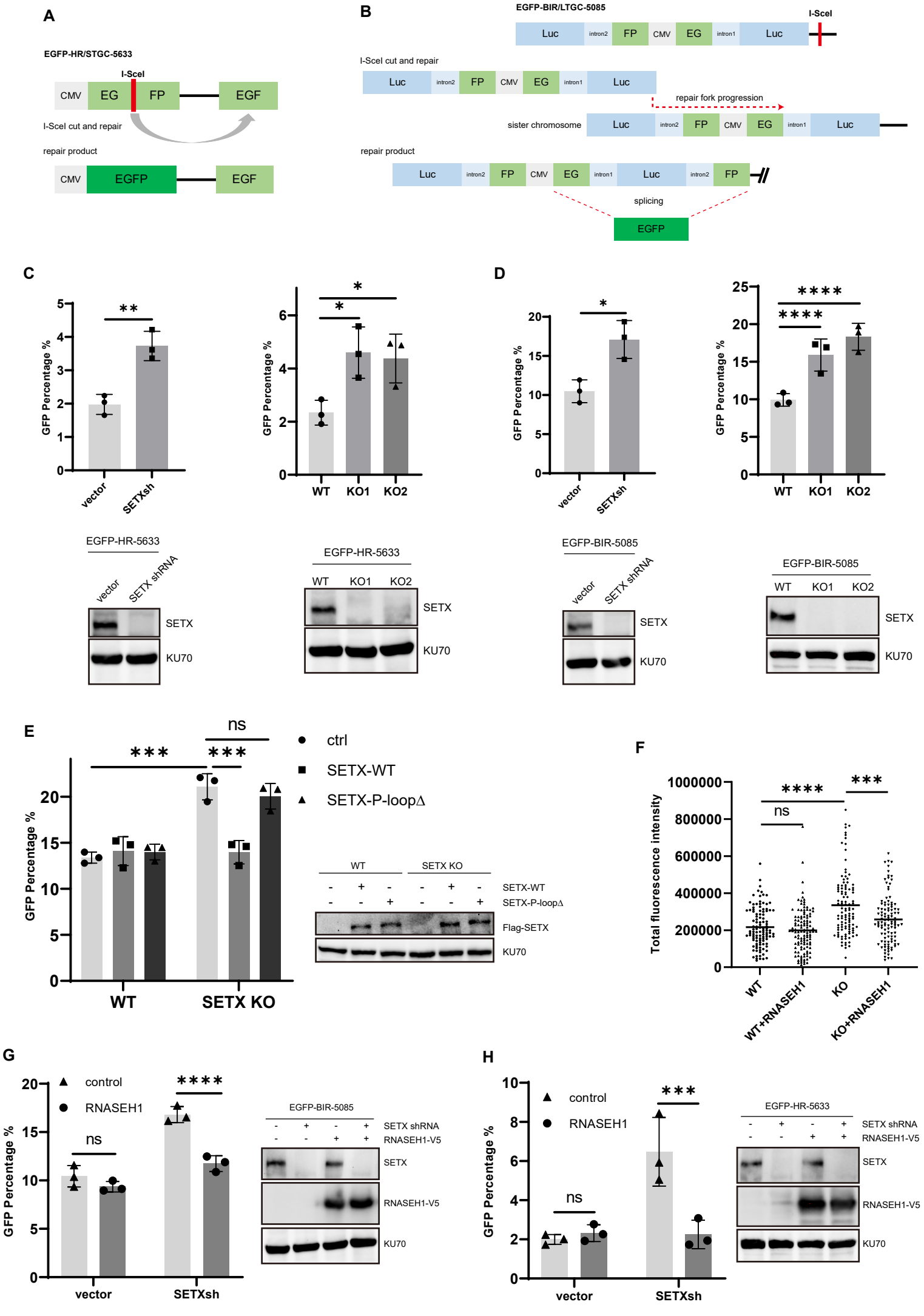
A
EGFP-HR/STGC-5633
I-SceI
CMV
EG
FP
EGF
I-SceI cut and repair
repair product
CMV
EGFP
EGF
B
EGFP-BIR/LTGC-5085
I-SceI
Luc
intron2
FP
CMV
EG
intron1
Luc
I-SceI cut and repair
repair fork progression
sister chromosome
repair product
splicing
EGFP
C
GFP Percentage %
vector
SETXsh
WT
KO1
KO2
EGFP-HR-5633
SETX shRNA
SETX
KU70
D
EGFP-BIR-5085
E
ctrl
SETX-WT
SETX-P-loopΔ
WT
SETX KO
Flag-SETX
F
Total fluorescence intensity
WT+RNASEH1
KO
KO+RNASEH1
G
control
RNASEH1
RNASEH1-V5
H

Fig 2

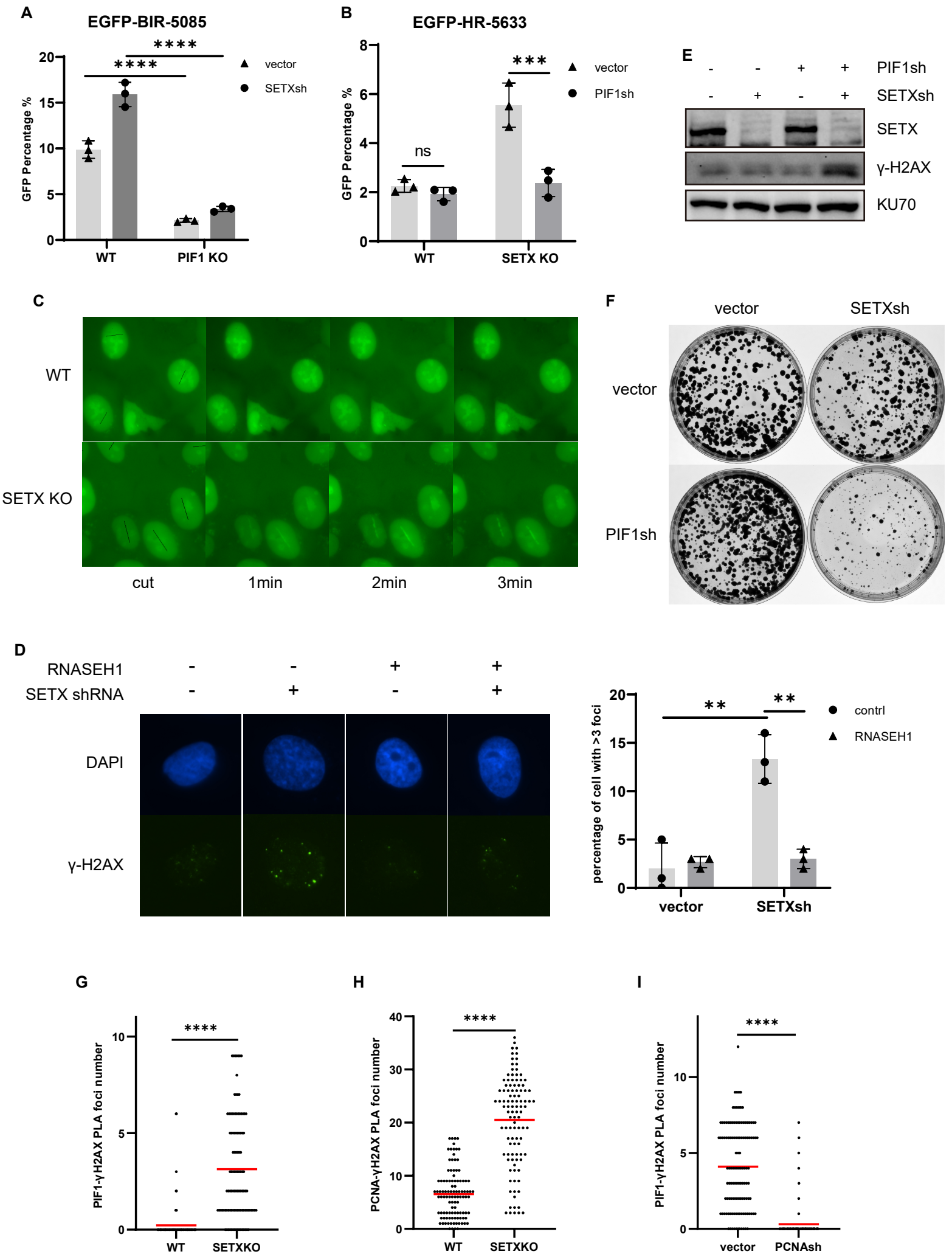
A
EGFP-BIR-5085
GFP Percentage %
****
****
vector
SETXsh
WT
PIF1 KO
B
EGFP-HR-5633
GFP Percentage %
***
ns
vector
PIF1sh
WT
SETX KO
E
PIF1sh
SETXsh
SETX
γ-H2AX
KU70
C
WT
SETX KO
cut
1min
2min
3min
F
vector
SETXsh
vector
PIF1sh
D
RNASEH1
SETX shRNA
DAPI
γ-H2AX
percentage of cell with >3 foci
**
**
contrl
RNASEH1
vector
SETXsh
G
PIF1-γH2AX PLA foci number
****
WT
SETXKO
H
PCNA-γH2AX PLA foci number
****
WT
SETXKO
I
PIF1-γH2AX PLA foci number
****
vector
PCNAsh

Fig 3

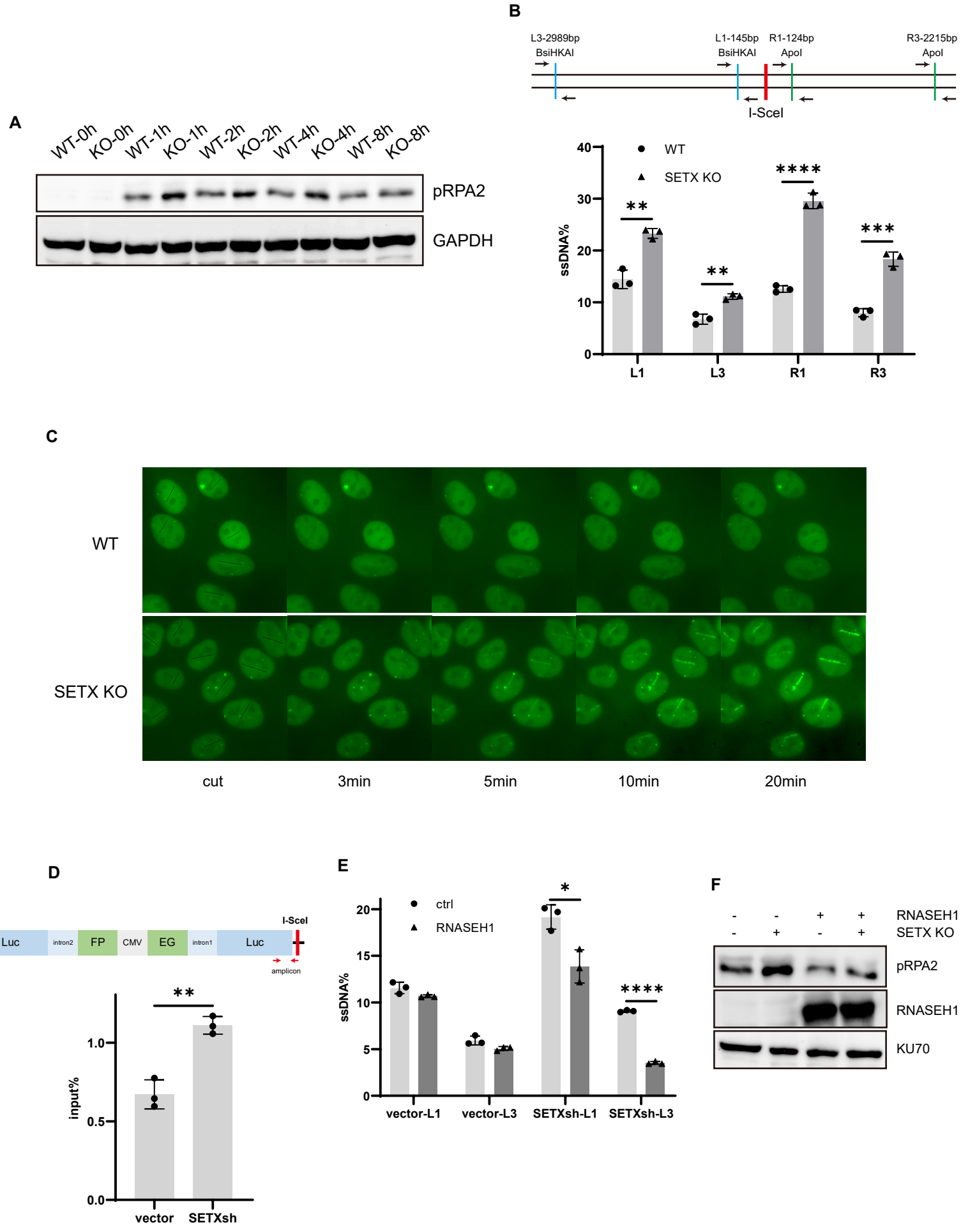
A
WT-0h
KO-0h
WT-1h
KO-1h
WT-2h
KO-2h
WT-4h
KO-4h
WT-8h
KO-8h
pRPA2
GAPDH
B
L3-2989bp
BsiHKAI
L1-145bp
BsiHKAI
R1-124bp
ApoI
R3-2215bp
ApoI
I-SceI
WT
SETX KO
ssDNA%
L1
L3
R1
R3
C
WT
SETX KO
cut
3min
5min
10min
20min
D
Luc
intron2
FP
CMV
EG
intron1
Luc
I-SceI
amplicon
input%
vector
SETXsh
E
ctrl
RNASEH1
ssDNA%
vector-L1
vector-L3
SETXsh-L1
SETXsh-L3
F
RNASEH1
SETX KO
pRPA2
RNASEH1
KU70

Fig 4

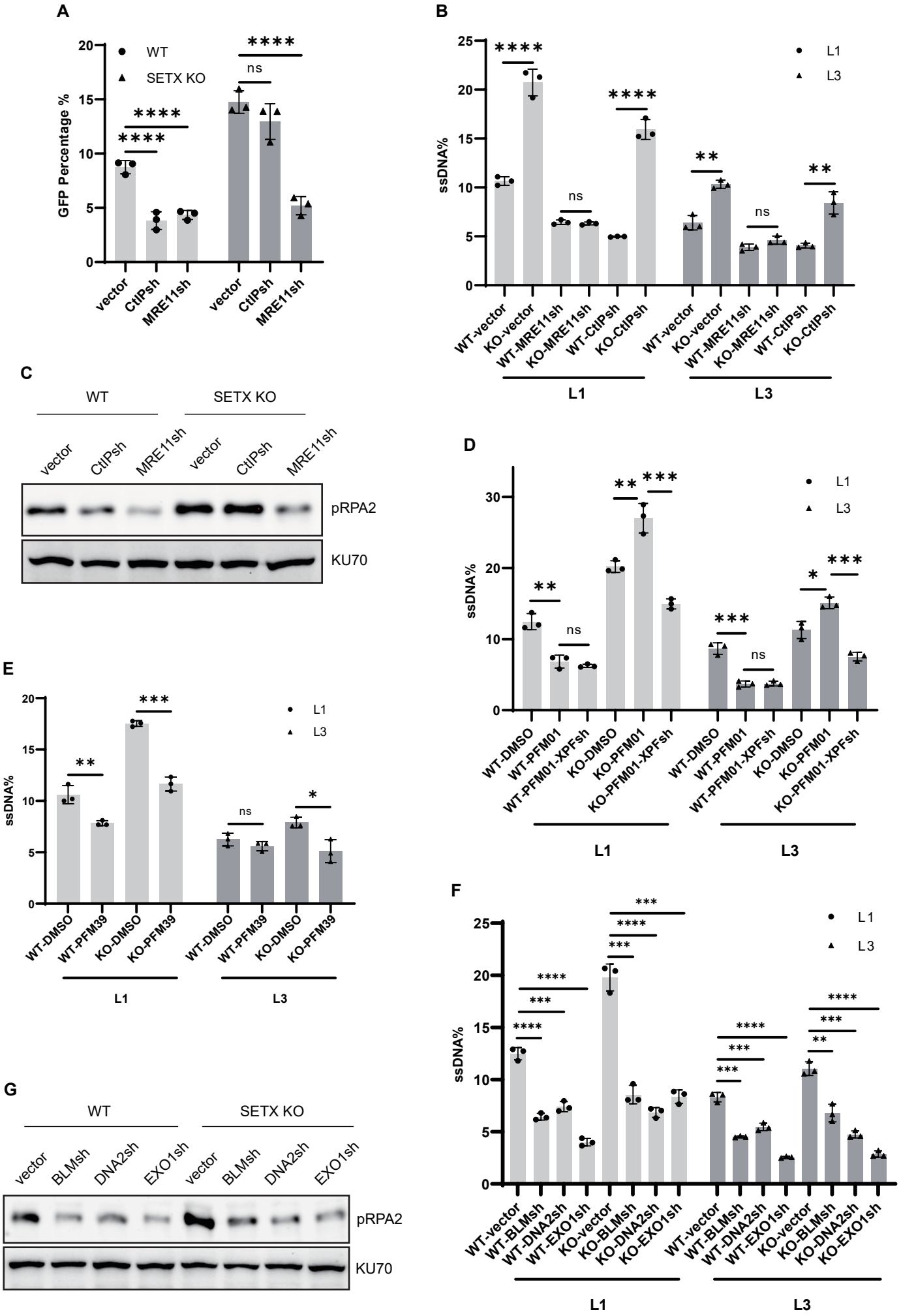
A
WT
SETX KO
GFP Percentage %
vector
CtlPsh
MRE11sh
B
L1
L3
ssDNA%
WT-vector
KO-vector
WT-MRE11sh
KO-MRE11sh
WT-CtlPsh
KO-CtlPsh
C
pRPA2
KU70
D
WT-DMSO
WT-PFM01
WT-PFM01-XPFsh
KO-DMSO
KO-PFM01
KO-PFM01-XPFsh
E
WT-PFM39
KO-PFM39
F
WT-BLMsh
WT-DNA2sh
WT-EXO1sh
KO-BLMsh
KO-DNA2sh
KO-EXO1sh
G
BLMsh
DNA2sh
EXO1sh

Fig 5

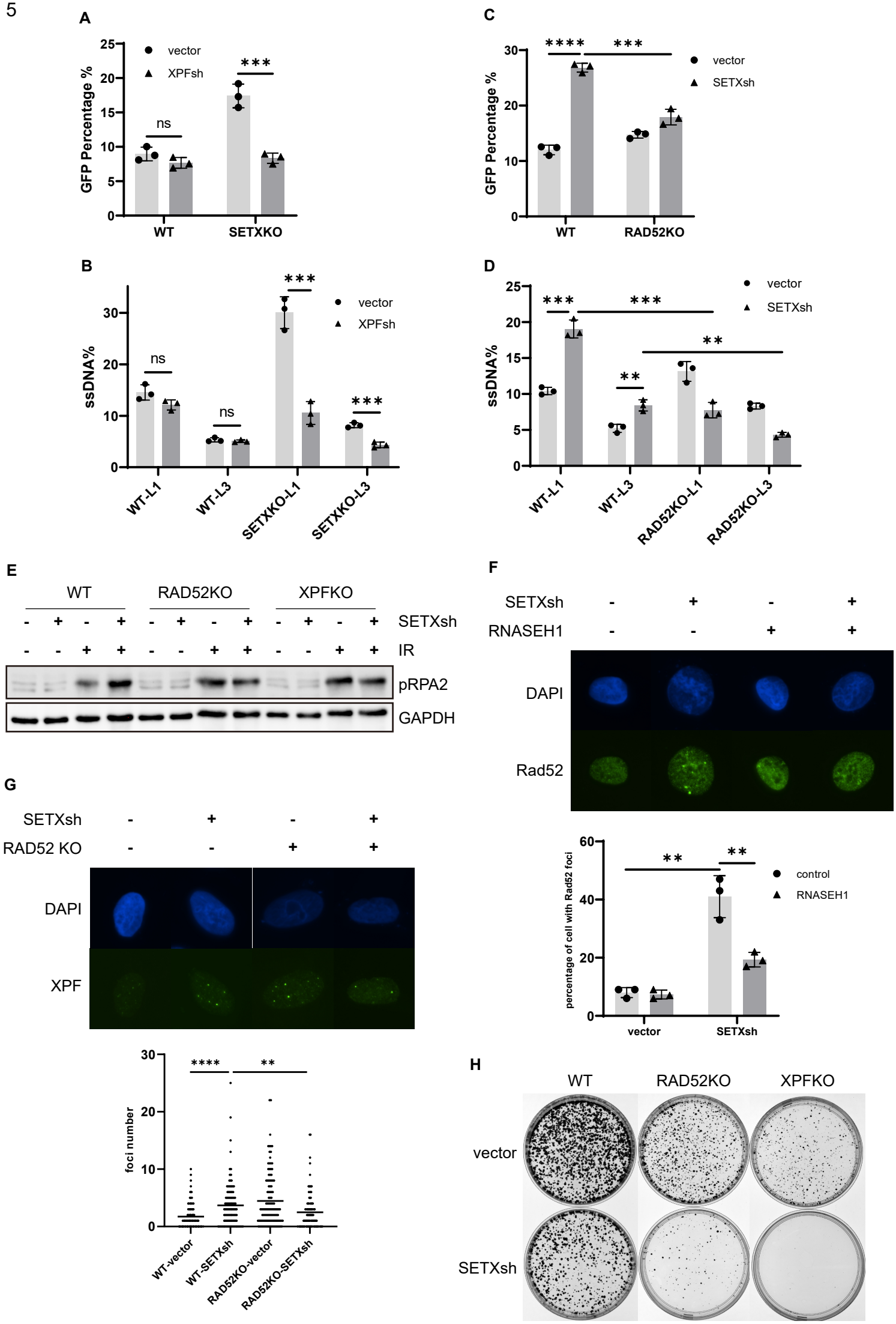
A
GFP Percentage %
vector
XPFsh
ns
***
WT
SETXKO
B
ssDNA%
vector
XPFsh
ns
ns
***
***
WT-L1
WT-L3
SETXKO-L1
SETXKO-L3
C
GFP Percentage %
****
***
vector
SETXsh
WT
RAD52KO
D
ssDNA%
vector
SETXsh
***
***
**
**
WT-L1
WT-L3
RAD52KO-L1
RAD52KO-L3
E
WT
RAD52KO
XPFKO
SETXsh
IR
pRPA2
GAPDH
F
SETXsh
RNASEH1
DAPI
Rad52
percentage of cell with Rad52 foci
control
RNASEH1
**
**
vector
SETXsh
G
SETXsh
RAD52 KO
DAPI
XPF
foci number
****
**
WT-vector
WT-SETXsh
RAD52KO-vector
RAD52KO-SETXsh
H
WT
RAD52KO
XPFKO
vector
SETXsh

Fig 6

A

	resolved	within reporter	outsite reporter	plasmid	frequency
WT	42	5	1	0	14.29%
KO	40	9	13	1	53.66%
WT+RNASEH1	48	2	2	3	14.58%
KO+RNASEH1	41	1	1	4	14.63%

C

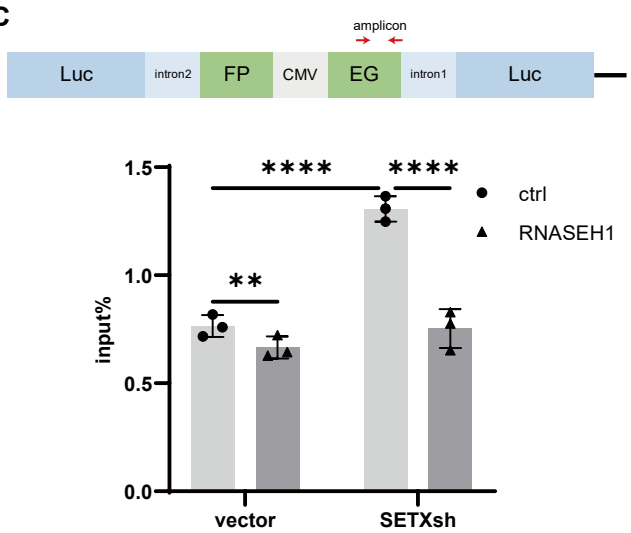

B

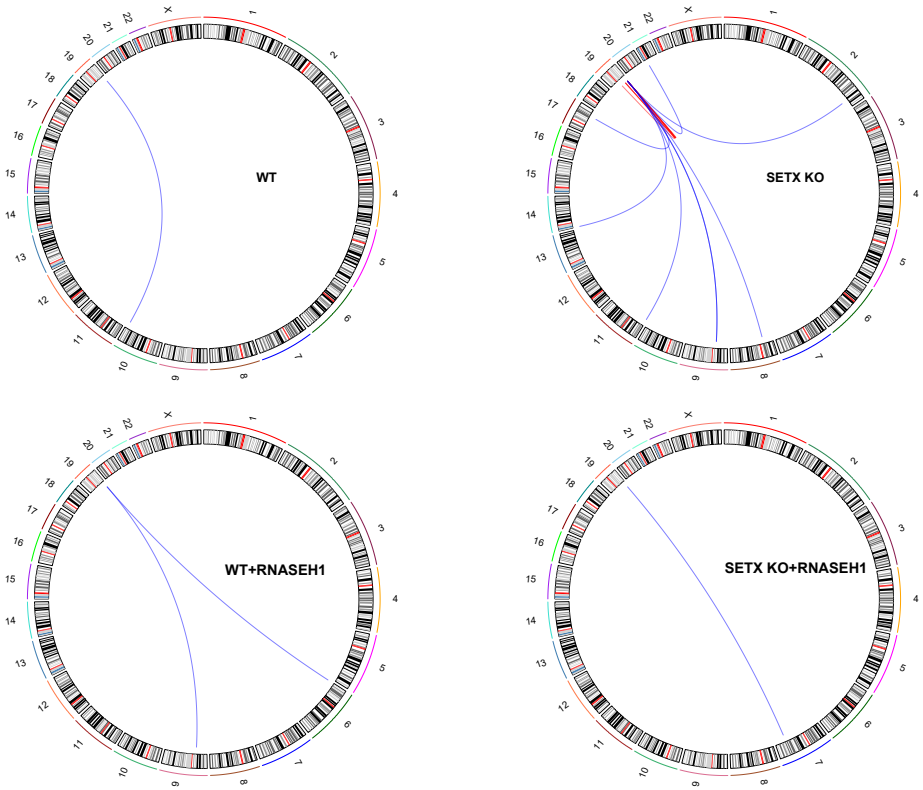

D

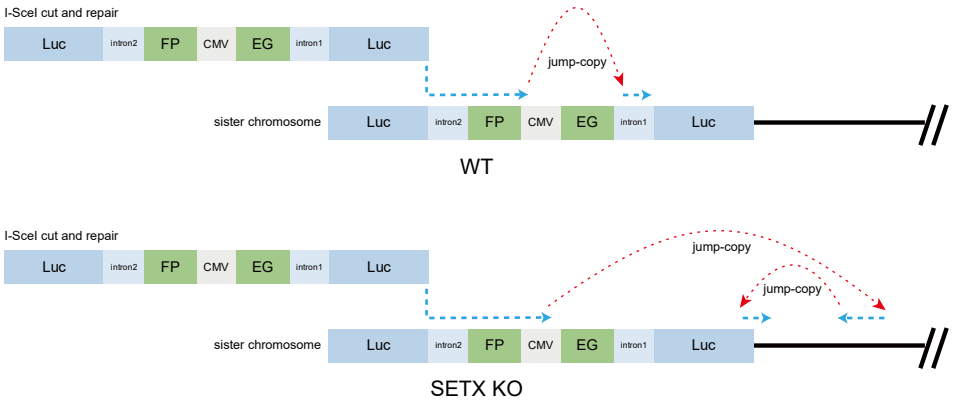

E

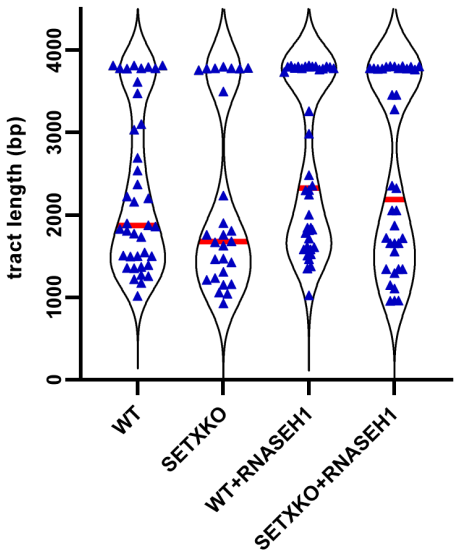

Fig 7

DSB repair in SETX-deficient cells

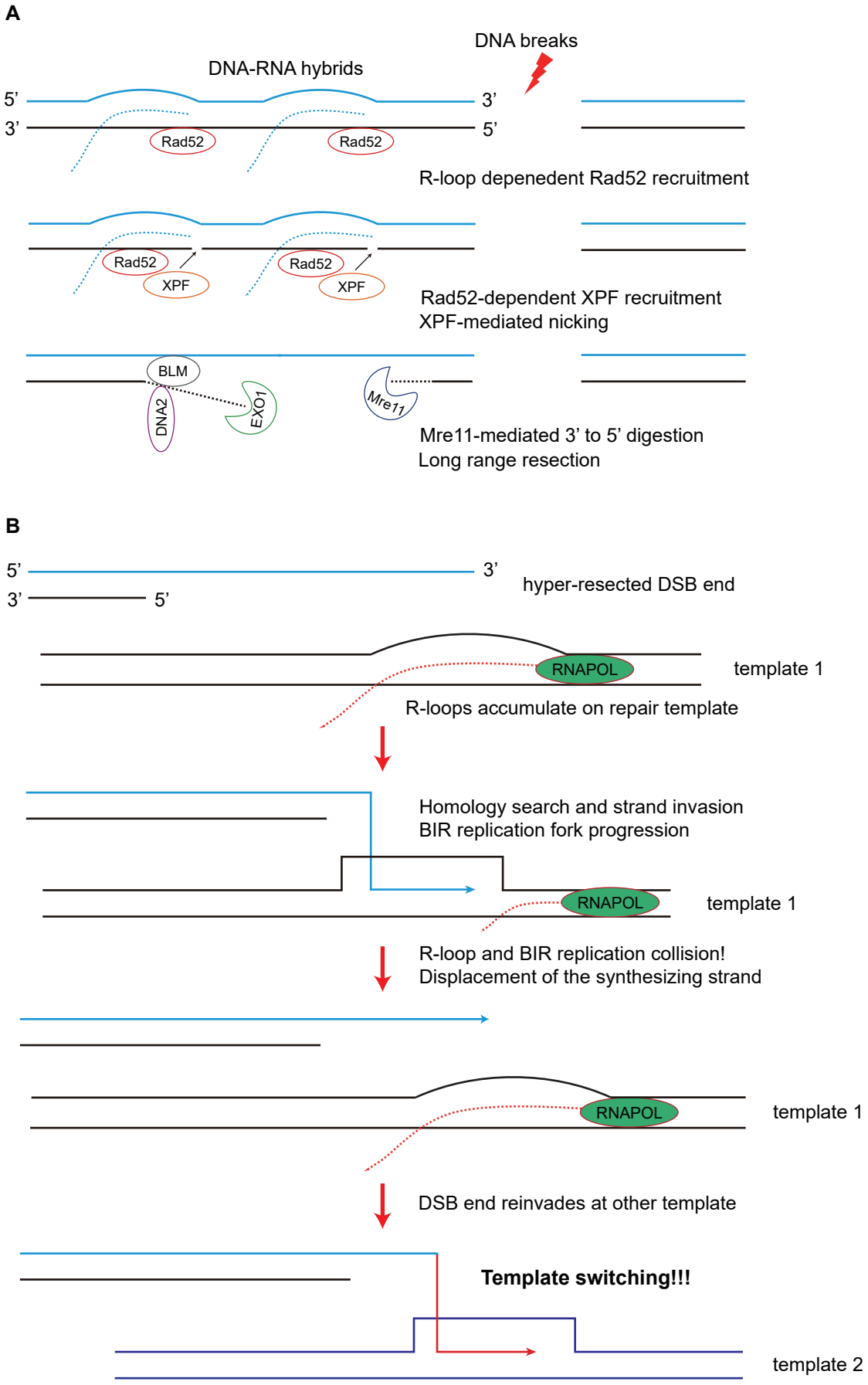

Fig S1

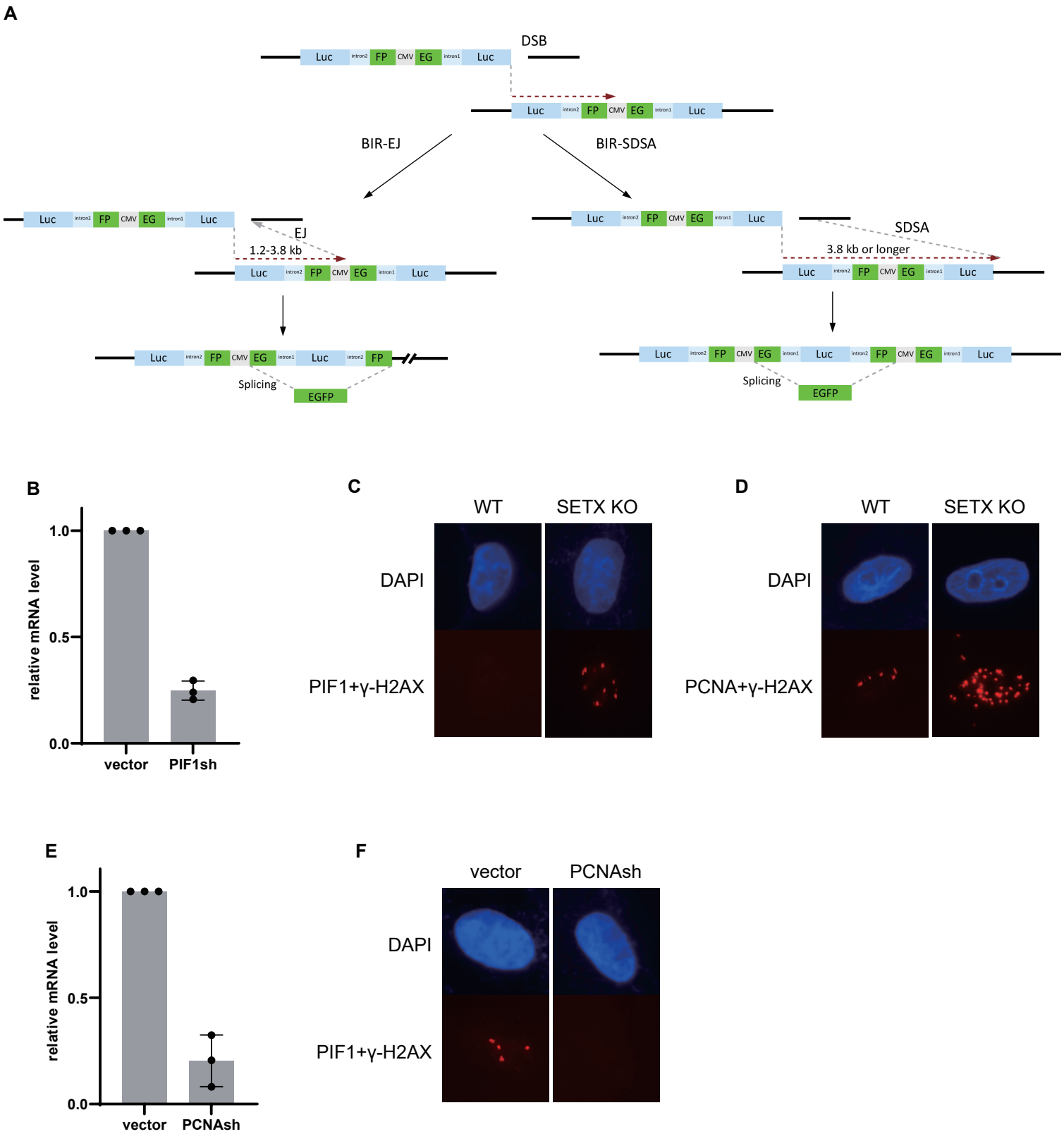

Fig S1 related to Fig 1 and Fig 2
Determining the dependence of the examined phenotypes on BIR-essential genes after SETX inactivation

A. Schematic drawing of repair products (BIR-EJ or BIR-SDSA) in EGFP-BIR-5085 reporter.
B. qPCR results showing the efficiency of PIF1 shRNA in U2OS EGFP-HR-5633 reporter cells.
C,D,F. Representative images of PLA assay between γ-H2AX and Flag-Pif1 or PCNA shown in Fig 2G,H,I.
E qPCR results showing the efficiency of PCNA shRNA in U2OS EGFP-HR-5085 reporter cells.

Fig S2

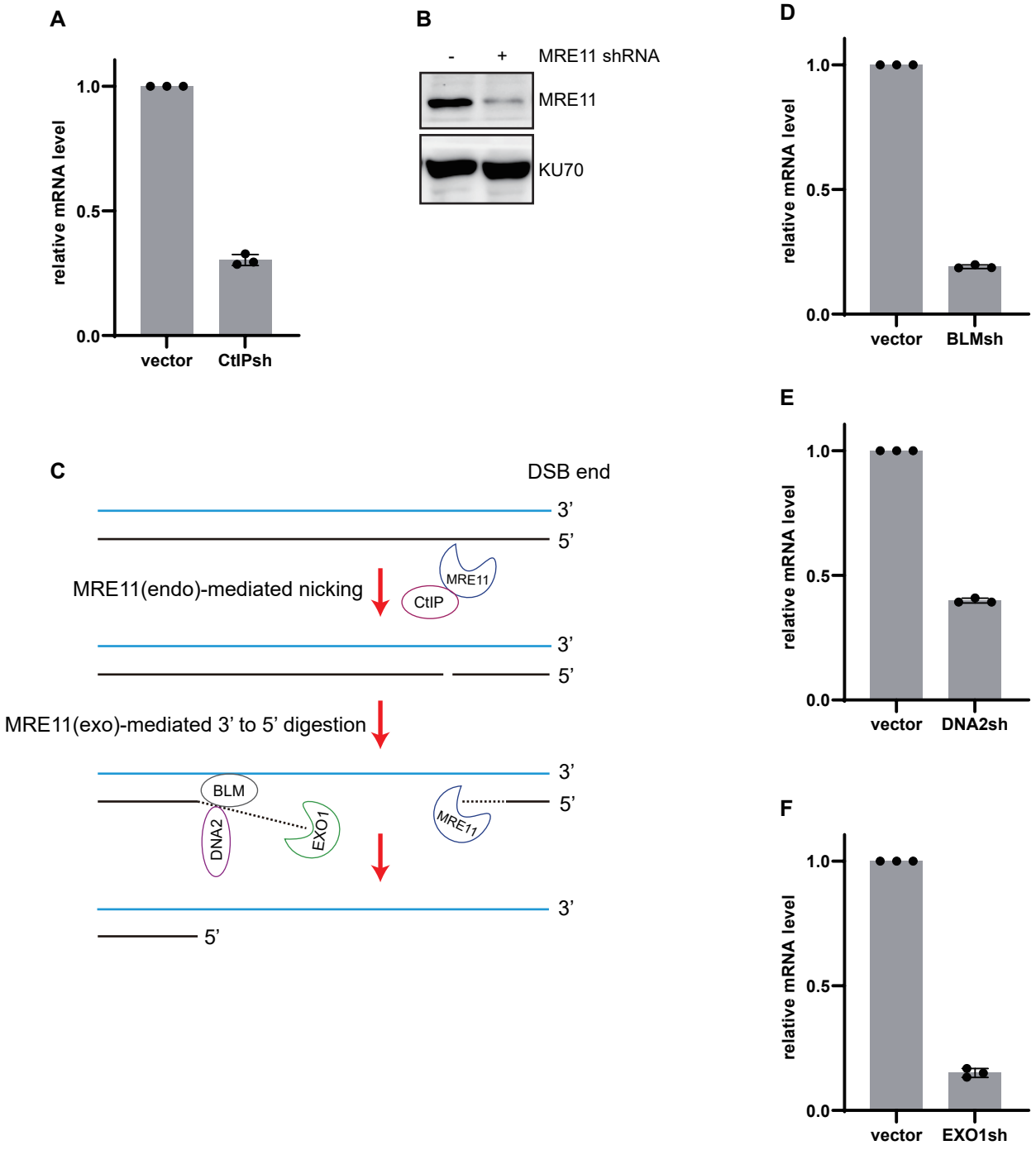

Fig S2 related to Fig 3
Determining the dependence on the genes required for canonical end resection pathway in SETX-deficient cells

A. qPCR results showing the efficiency of CtIP shRNA in U2OS EGFP-BIR-5085 reporter cells.
B. Western blotting showing the efficiency of MRE11 shRNA in U2OS EGFP-BIR-5085 reporter cells.
C. Schematic drawing of the classical end resection pathway.
D,E,F. qPCR results showing the efficiency of BLM shRNA, DNA2 shRNA, and EXO1 shRNA in U2OS EGFP-BIR-5085 reporter cells.

Fig S3

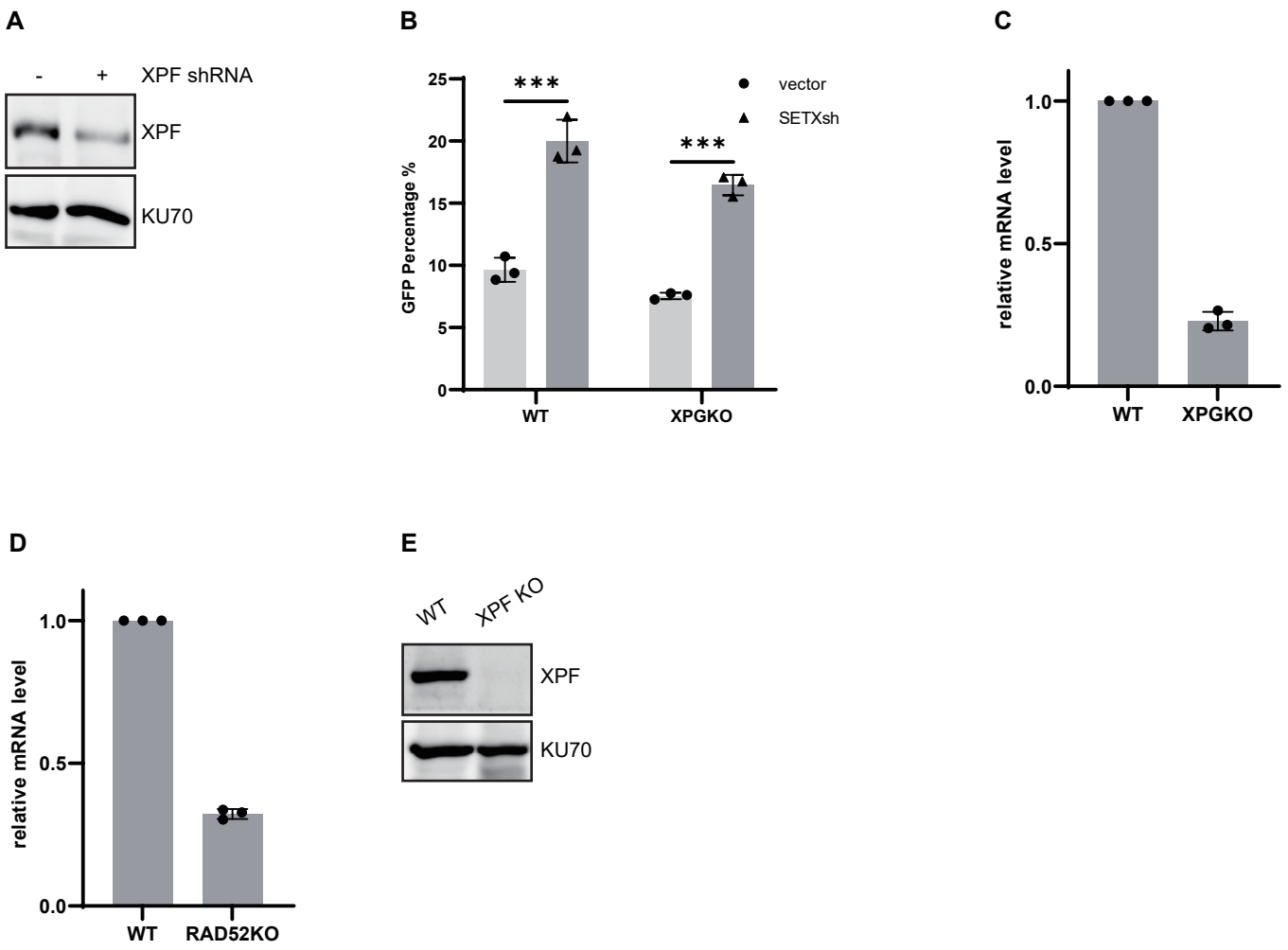

Fig S3 related to Fig 5

Determining the BIR dependence on XPF/RAD52 in SETX-deficient cells

A. U2OS WT and XPG-KO EGFP-BIR-5085 reporter cells were infected with SETX shRNA or vector. Three days after infection, cells were infected with I-SceI-expressing lentivirus to induce DSBs. The percentage of EGFP-positive cells was quantified by FACS analysis five days after I-SceI infection.

B. qPCR results showing the efficiency of XPG knockout in U2OS EGFP-BIR-5085 reporter cells.

C. Western blotting showing the efficiency of XPF shRNA in U2OS EGFP-BIR-5085 reporter cells.

D. qPCR results showing the efficiency of RAD52 knockout in U2OS EGFP-BIR-5085 reporter cells.

E. Western blotting showing the efficiency of XPF knockout in U2OS EGFP-BIR-5085 reporter cells.

Fig S4

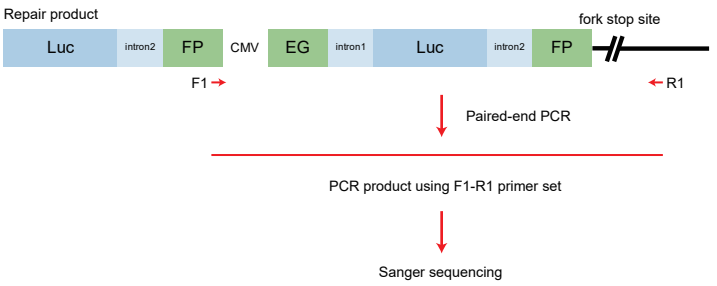

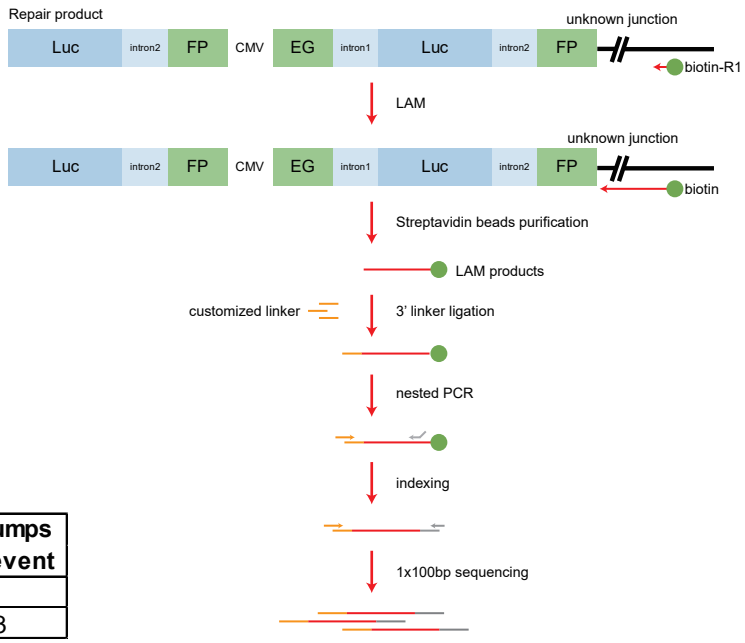

C

	total events	events resolved by PCR analysis	events with local jumps	local jumps times/event
WT	42	42	5	1
SETX-KO	41	17	7	1-3

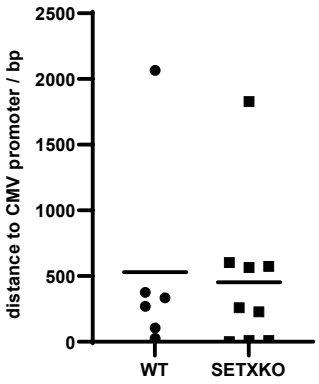

Fig S4 related to Fig 6

Development of LAM-HTGTS to identify the sequences at the repair junctions of the BIR products in U2OS EGFP-BIR-5085 reporter cells.

A. Schematic drawing of the PCR analysis assay in U2OS EGFP-BIR-5085 reporter cells.

B. Schematic drawing of the LAM-HTGTS assay in U2OS EGFP-BIR-5085 reporter cells.

C. Summary of the repair products which are resolved by the PCR analysis assay.

D. Summary of the distance between the first jumping site and the CMV promoter in the BIR jumping events. If the jumping happens within CMV promoter, the distance is recorded as 0 bp. Black lines mark the mean value.

Fig S5

A

a Local jumping and end joining to the right side of DSB

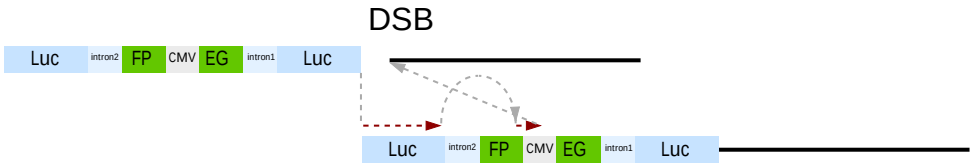

b Jumping outside and end joining to the right side of DSB

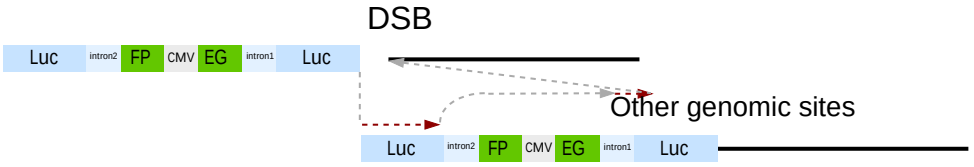

c Jumping outside

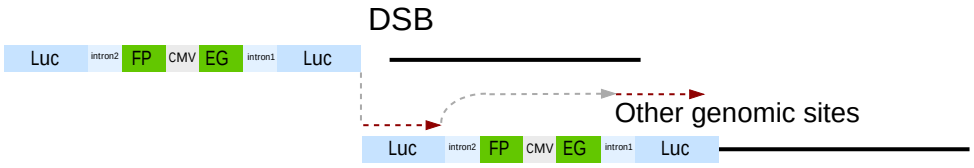

B R-loop cleavage by XPF and XPG

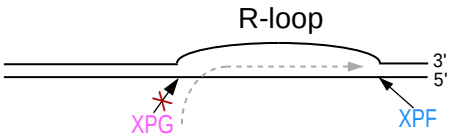

Putative XPF and XPG cleavage sites

Fig S5 LAM-HTGTS application and XPF/XPG cleavage pattern on the R-loop substrate.
A. Different types of template switching during BIR scored by the EGFP-BIR-5085 reporter: a, local jumping within the BIR reporter; b, long-distance jumping to the genomic sites outside of the BIR reporter region with BIR completed by end joining back to the original cleavage site; c, long-distance jumping to the genomic sites outside of the BIR reporter region, causing translocation to other genomic sites.
B. Schematic drawing of the putative XPF and XPG cleavage sites on R-loop-associated DSB ends to initiate end resection.

Fig S6

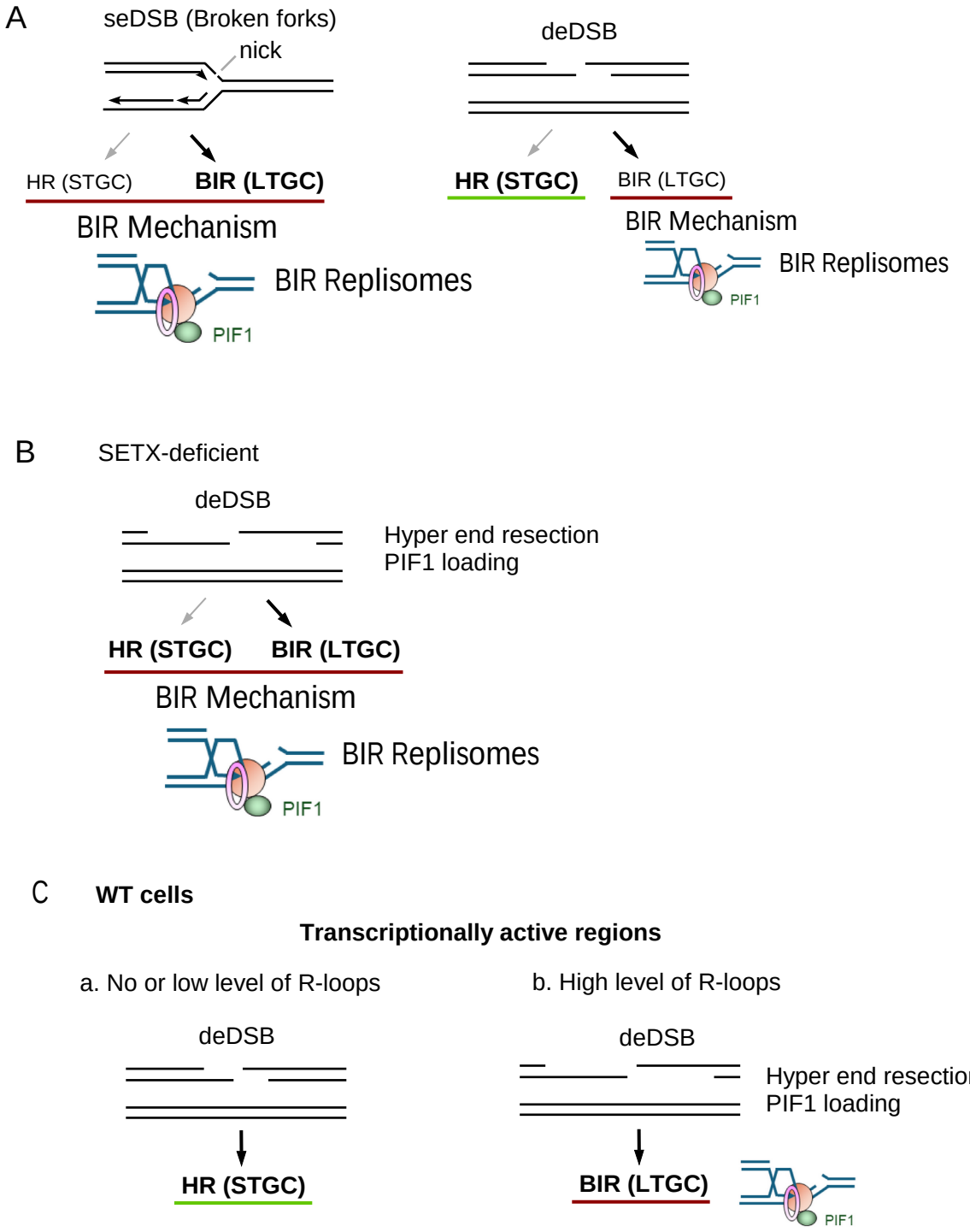

Fig S6 SETX and R-loop modulate DSB repair pathway choice.
A. Models showing BIR activation at seDSB on broken forks (left) and at deDSB (right).
B. Models showing BIR activation at deDSB when SETX is deficient.
C. Models showing how R-loop causes BIR activation at deDSB.

Fig S7

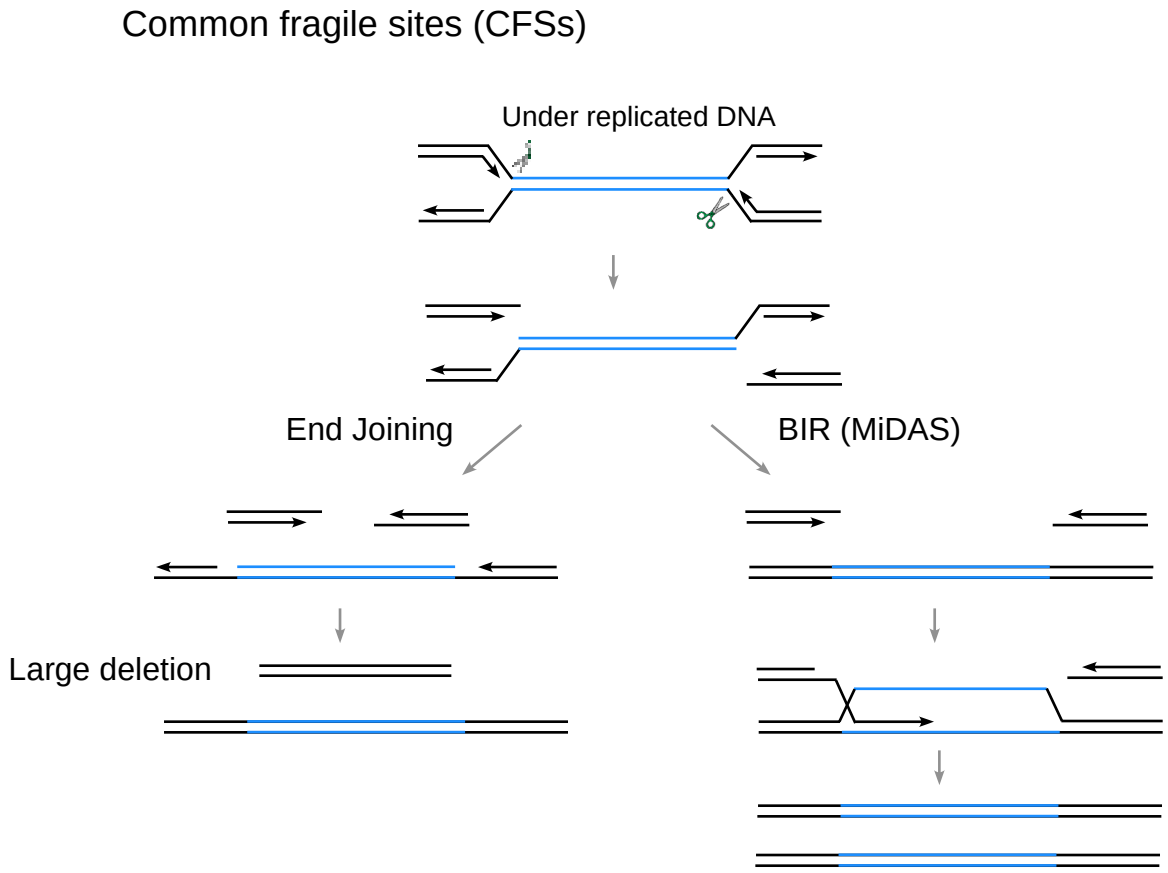

Fig S7 Models showing BIR prevents large deletions at CFSs through MiDAS.
Schematic drawing of repair products by end joining and BIR to repair DSBs at CFSs in mitosis.

Fig S8

A **Dysregulation of end resection**

DSB accumulated with R-loop

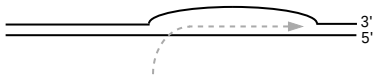

Promote hyper end resection:

SETX loss: promotes RAD52-XPF hyper resection pathway

EXOSC10 loss: enhances transcription-dependent end resection

Inhibit end resection:

Inhibition of MRE11 complex

Inhibition of DNA2, BLM, EXO1

B **Dysregulation of homologous recombination**

Stimulate recombination: SETX loss

Inhibit HR

a. Inhibition of end resection

b. Inhibition of removal of RNA hybrids on 3' DNA overhangs

c. Inhibition of loading of RPA, RAD51 and other HR proteins to 3' ssDNA overhangs

C SETX deficiency

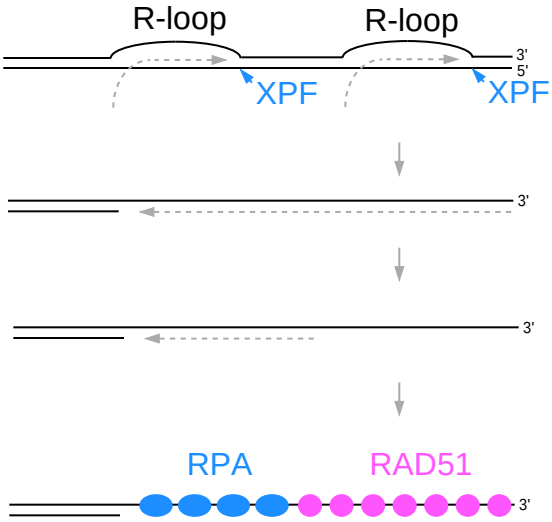

Hyper end resection

de novo transcription on 3' overhangs:
protecting 3' ssDNA overhangs

Removal of hybrids on 3' overhangs
by other RNA/DNA resolvases

Loading of RPA and RAD51 for strand invation

Fig S8 Summary of the effects of R-loop on DSB repair.
A. Different effects on end resection by R-loop accumulation at DSBs due to defects in various R-loop resolving mechanisms.
B. R-loop accumulation at DSB ends, due to defects in various R-loop resolving mechanisms, causes dysregulation of HR at different stages.
C. The model showing how SETX-deficiency-induced R-loop accumulation contributes to end resection without affecting other steps, thus leading to hyperrecombination.